1-1-2012

Comparisons of observed and modeled OH and HO 2 concentrations during the ambient measurement period of the HOxComp field campaign

Y Kanaya
Japan Agency for Marine-Earth Science & Technology

A Hofzumahaus
Forschungszentrum Jiilich, Germany

H-P Dorn
Forschungszentrum Jiilich, Germany

T Brauers
Forschungszentrum Jiilich, Germany

H Fuchs
Forschungszentrum Jiilich, Germany

See next page for additional authors

Comparisons of observed and modeled OH and HO 2 concentrations during the ambient measurement period of the HOxComp field campaign

Abstract

A photochemical box model constrained by ancillary observations was used to simulate OH and HO 2 concentrations for three days of ambient observations during the HOxComp field campaign held in Jülich, Germany in July 2005. Daytime OH levels observed by four instruments were fairly well reproduced to within 33% by a base model run (Regional Atmospheric Chemistry Mechanism with updated isoprene chemistry adapted from Master Chemical Mechanism ver. 3.1) with high R 2 values (0.72-0.97) over a range of isoprene (0.3-2 ppb) and NO (0.1-10 ppb) mixing ratios. Daytime HO 2(*) levels, reconstructed from the base model results taking into account the sensitivity toward speciated RO 2 (organic peroxy) radicals, as recently reported from one of the participating instruments in the HO 2 measurement mode, were 93% higher than the observations made by the single instrument. This also indicates an overprediction of the HO 2 to OH recycling. Together with the good model-measurement agreement for OH, it implies a missing OH source in the model. Modeled OH and HO 2(*) could only be matched to the observations by addition of a strong unknown loss process for HO 2(*) that recycles OH at a high yield. Adding to the base model, instead, the recently proposed isomerization mechanism of isoprene peroxy radicals (Peeters and Müller, 2010) increased OH and HO 2(*) by 28% and 13% on average. Although these were still only 4% higher than the OH observations made by one of the instruments, larger overestimations (42-70%) occurred with respect to the OH observations made by the other three instruments. The overestimation in OH could be diminished only when reactive alkanes (HC8) were solely introduced to the model to explain the missing fraction of observed OH reactivity. Moreover, the overprediction of HO 2(*) became even larger than in the base case. These analyses imply that the rates of the isomerization are not readily supported by the ensemble of radical observations. One of the measurement days was characterized by low isoprene concentrations (∼0.5 ppb) and OH reactivity that was well explained by the observed species, especially before noon. For this selected period, as opposed to the general behavior, the model tended to underestimate HO 2(*). We found that this tendency is associated with high NO x concentrations, suggesting that some HO 2 production or regeneration processes under high NO x conditions were being overlooked; this might require revision of ozone production regimes.

Keywords

measurement, ambient, during, concentrations, 2, ho, campaign, oh, field, modeled, observed, comparisons, period, hoxcomp

Disciplines

Life Sciences | Physical Sciences and Mathematics | Social and Behavioral Sciences

Publication Details

Kanaya, Y., Hofzumahaus, A., Dorn, H., Brauers, T., Fuchs, H., Holland, F., Rohrer, F., Bohn, B., Tillmann, R., Wegener, R., Wahner, A., Kajii, Y., Miyamoto, K., Nishida, S., Watanabe, K., Yoshino, A., Kubistin, D. C., Martinez, M., Rudolf, M., Harder, H., Berresheim, H., Elste, T., Plass-Dulmer, C., Stange, G., Kleffmann, J., Elshorbany, Y. & Schurath, U. (2012). Comparisons of observed and modeled OH and HO 2 concentrations during the ambient measurement period of the HOxComp field campaign. Atmospheric Chemistry and Physics, 12 (5), 2567-2585.

Authors

Y Kanaya, A Hofzumahaus, H-P Dorn, T Brauers, H Fuchs, F Holland, F Rohrer, B Bohn, R Tillmann, Rebekah Wegener, A Wahner, Y Kajii, K Miyamoto, S Nishida, K Watanabe, A Yoshino, Dagmar C. Kubistin, M

Atmos. Chem. Phys., 12, 2567–2585, 2012
www.atmos-chem-phys.net/12/2567/2012/
doi:10.5194/acp-12-2567-2012

Atmospheric Chemistry and Physics

Comparisons of observed and modeled OH and HO_2 concentrations during the ambient measurement period of the HO_xComp field campaign

Y. Kanaya[1], A. Hofzumahaus[2], H.-P. Dorn[2], T. Brauers[2], H. Fuchs[2], F. Holland[2], F. Rohrer[2], B. Bohn[2], R. Tillmann[2], R. Wegener[2], A. Wahner[2], Y. Kajii[3], K. Miyamoto[3], S. Nishida[3,*], K. Watanabe[3], A. Yoshino[3,], D. Kubistin[4,***], M. Martinez[4], M. Rudolf[4], H. Harder[4], H. Berresheim[5,****], T. Elste[5], C. Plass-Dülmer[5], G. Stange[5], J. Kleffmann[6], Y. Elshorbany[6,*****], and U. Schurath[7]**

[1]Research Institute for Global Change (formerly FRCGC), Japan Agency for Marine-Earth Science and Technology, Yokohama 236-0001, Japan
[2]Forschungszentrum Jülich, IEK-8: Troposphäre, 52425 Jülich, Germany
[3]Tokyo Metropolitan University, Department of Applied Chemistry, Tokyo 192-0397, Japan
[4]Max Planck Institute for Chemistry, Atmospheric Chemistry Department, 55020 Mainz, Germany
[5]Deutscher Wetterdienst, Meteorologisches Observatorium, 82383 Hohenpeissenberg, Germany
[6]Bergische Universität Wuppertal, 42097 Wuppertal, Germany
[7]Karlsruhe Institute of Technology (KIT), IMK-AAF, 76021 Karlsruhe, Germany
*now at: Gifu University, Gifu 501-1193, Japan
**now at: Tokyo University of Agriculture and Technology, Tokyo 183-8538, Japan
***now at: University of Wollongong, School of Chemistry, Wollonong, NSW, Australia
****now at: National University of Ireland Galway, Department of Physics, Galway, Ireland
*****now at: Max Planck Institute for Chemistry, Atmospheric Chemistry Department, 55020 Mainz, Germany

Correspondence to: Y. Kanaya (yugo@jamstec.go.jp)

Received: 21 September 2011 – Published in Atmos. Chem. Phys. Discuss.: 26 October 2011
Revised: 11 February 2012 – Accepted: 13 February 2012 – Published: 7 March 2012

Abstract. A photochemical box model constrained by ancillary observations was used to simulate OH and HO_2 concentrations for three days of ambient observations during the HO_xComp field campaign held in Jülich, Germany in July 2005. Daytime OH levels observed by four instruments were fairly well reproduced to within 33 % by a base model run (Regional Atmospheric Chemistry Mechanism with updated isoprene chemistry adapted from Master Chemical Mechanism ver. 3.1) with high R^2 values (0.72–0.97) over a range of isoprene (0.3–2 ppb) and NO (0.1–10 ppb) mixing ratios. Daytime HO_2(*) levels, reconstructed from the base model results taking into account the sensitivity toward speciated RO_2 (organic peroxy) radicals, as recently reported from one of the participating instruments in the HO_2 measurement mode, were 93 % higher than the observations made by the single instrument. This also indicates an overprediction of the HO_2 to OH recycling. Together with the good model-measurement agreement for OH, it implies a missing OH source in the model. Modeled OH and HO_2(*) could only be matched to the observations by addition of a strong unknown loss process for HO_2(*) that recycles OH at a high yield. Adding to the base model, instead, the recently proposed isomerization mechanism of isoprene peroxy radicals (Peeters and Müller, 2010) increased OH and HO_2(*) by 28 % and 13 % on average. Although these were still only 4 % higher than the OH observations made by one of the instruments, larger overestimations (42–70 %) occurred with respect to the OH observations made by the other three instruments. The overestimation in OH could be diminished only when reactive alkanes (HC8) were solely introduced to the model to explain the missing fraction of observed OH reactivity. Moreover, the overprediction of HO_2(*) became even larger than in the base case. These analyses imply that the rates of the isomerization are not readily supported by the ensemble of radical observations. One of the measurement days was characterized by low isoprene concentrations (~0.5 ppb) and OH reactivity that was well explained by the observed species, especially before noon. For this selected

period, as opposed to the general behavior, the model tended to underestimate HO_2(*). We found that this tendency is associated with high NO_x concentrations, suggesting that some HO_2 production or regeneration processes under high NO_x conditions were being overlooked; this might require revision of ozone production regimes.

1 Introduction

Reactions of OH and HO_2 radicals in the troposphere constitute the basis of the chemical mechanisms explaining photochemical ozone production and formation of acidic species. Fundamental radical reactions also control the behaviors of important chemical species related to global climate change (e.g., methane). Comparisons of modeled and observed tropospheric OH and HO_2 radical concentrations have served as effective tests of our current understanding of tropospheric chemistry mechanisms. Past comparisons near the Earth's surface and in the air above led to the identification of new processes essential to the budget of HO_x ($OH + HO_2$) radicals; these processes had previously been missing from our knowledge (e.g., acetone photolysis, Wennberg et al., 1998). Although they may not lead to an immediate clarification of processes, the accumulation of these comparisons at multiple sites is important for the identification of common tendencies. For example, HO_2 concentrations are overestimated in clean coastal regions (Sommariva et al., 2004; Kanaya et al., 2002, 2007a), and this assists systematic surveying of the processes responsible for the discrepancies. Recent observations revealed that OH concentrations under high volatile organic compound (VOC) and low NO_x conditions were systematically larger than the modeled concentrations. Hofzumahaus et al. (2009) and Lu et al. (2012) suggested that unidentified processes converting RO_2 to HO_2 and HO_2 to OH have an effect in a rural area in the Pearl River Delta (PRD), China. Martinez et al. (2010), Kubistin et al. (2010), and Ren et al. (2008) found that OH and HO_2 radical concentrations measured by aircraft over Suriname and the eastern United States were higher than those modeled in the planetary boundary layer when accompanied by high isoprene concentrations emitted from the terrestrial biosphere. Recently, three-dimensional chemical transport models (Peeters and Müller, 2010; Stavrakou et al., 2010; Archibald et al., 2010) explained the high radical concentration levels observed in regions of biosphere influence at least qualitatively using isomerization of isoprene peroxy radicals, basically as proposed by theoretical studies (Peeters et al., 2009; Peeters and Müller, 2010). Similar underestimation by model calculations has been reported for OH in tropical forests (Whalley et al., 2011; Stone et al. 2011; Pugh et al., 2010) and in temperate forests (Carslaw et al., 2001; Tan et al., 2001).

Recent measurements of OH reactivity have added a new dimension to the diagnosis of the HO_x chemistry. A fraction of the observed reactivity is sometimes left unexplained by the sum of reactivities contributed from known gas species present in the atmosphere, suggesting the existence of unmeasured species that contribute to OH loss (Di Carlo et al., 2004; Sadanaga et al., 2005; Yoshino et al., 2006). Thus, the knowledge of a robust set of reactions that reasonably explain both OH reactivity and radical concentrations is still an open issue. The studies focusing on this issue contribute to a better understanding, and improvements in the predictive capabilities of various atmospheric phenomena that are based on fundamental radical chemistry.

Because only a few research groups have performed tropospheric OH and HO_2 observations, in the past, HO_x measurements were normally made by a single instrument during individual campaigns, and such observations were compared with theoretical values. The HO_xComp field campaign (Schlosser et al., 2009; Fuchs et al., 2010) was an exceptional and unique opportunity: OH and HO_2 concentrations were measured with multiple instruments, and thus more reliable comparisons with model results could be made. Schlosser et al. (2009) reported that ambient OH levels measured by four instruments correlated strongly (R^2 ranged from 0.75 to 0.96), and that the slopes of pairwise linear regressions were between 1.06 and 1.69 (with negligible intercepts); this can be partly explained by the stated instrumental accuracies. They argue that sampling inhomogeneities and calibration problems have contributed to the discrepancies. Fuchs et al. (2010) stated that ambient daytime HO_2 levels, measured by three instruments, correlated with each other even more strongly (R^2 ranged from 0.92 to 0.98), with a similar range of linear-regression slopes (1.19–1.69) and with small intercepts. However, a systematic sensitivity difference, which was dependent on the amount of water vapor and was noticed in comparisons with chamber air, would also affect ambient measurements. Again, the slope values can only be partly explained by the combined 1σ accuracies of the calibrations. Here, we evaluate the degrees of agreement between the observed OH and HO_2 concentrations and theoretical values predicted using a photochemical box model. By changing the set of reactions used in the model, we examine the potential impact of the isomerization of isoprene peroxy radicals. We also study the tendency, found in measurements of HO_2 levels with three instruments, for models to underestimate HO_2 levels at high NO levels. Outlines of the experiments are described briefly in Sect. 2, followed by a detailed explanation of the model simulations in Sect. 3. Results and discussion are given in Sect. 4. In another paper (Elshorbany et al., 2012), a detailed analysis of the HO_x radical budgets, secondary radical balance and turnover rates as well as the impact of HONO on the radical chemistry on 10 July 2005, using the master chemical mechanism (MCM), is presented.

2 Experimental and ambient air conditions

HO_xComp was designed to compare HO_x measurements performed by different instruments in a blind intercomparison under well characterized atmospheric chemical conditions. Details of HO_xComp have been described by Schlosser et al. (2009) and Fuchs et al. (2010). In this paper, daytime data during the ambient observation period (9, 10, and 11 July 2005) are analyzed in detail. The measurement site on the campus of Forschungszentrum Jülich (50°54′33″ N, 06°24′44′ E) is located in a mixed deciduous forest (Stetternicher Forst) in a rural area close to Jülich, Germany. The forest area around the campus has an extension of about 1–2 km in the wind direction encountered during the three days, and consists mainly of oak, birch, and beech.

A chemical ionization mass spectrometry (CIMS) instrument from Deutscher Wetterdienst (DWD) measured OH levels (Berresheim et al., 2000; Rohrer and Berresheim, 2006). Three laser-induced fluorescence (LIF) instruments, from the Frontier Research Center for Global Change (FRCGC) (Kanaya et al., 2001; Kanaya and Akimoto, 2002, 2006), Forschungszentrum Jülich (FZJ) (Lu et al., 2012; Fuchs et al., 2011), and the Max Planck Institute (MPI) (Martinez et al., 2010), measured OH and HO_2 concentrations. A tandem chamber with multi-pass for laser excitation was employed for the MPI instrument, while a dual chamber with single-pass for laser excitation was used for the FZJ instrument. The FRCGC instrument employed a single chamber with single-pass for laser excitation. For more details, see Schlosser et al. (2009). Each instrument was calibrated by its own system. The instruments were housed in containers and set up on the paved area between the institute building and the SAPHIR chamber. The instruments were separated by 2.7–4.5 m (see Fig. 1 of Schlosser et al., 2009). All the OH and HO_2 measurements were made by sampling ambient air at approximately equal heights (3.5 m) above the ground. The detection limits and uncertainties for the OH and HO_2 observations are summarized in Table 1. The HO_2/OH ratio for the FRCGC instrument, where OH and HO_2 were detected in the same single cell alternately and thus systematic uncertainties in OH and HO_2 measurements arising from calibration are common and cancel out, had a smaller uncertainty, ±6 % (1σ), estimated from the temporal variations in the HO_2-to-OH conversion efficiency determined during the calibrations for the whole campaign period. The OH and HO_2 data without quality flags (used as markers to indicate "not valid" by each group) were averaged for 10-min intervals and used for the analysis. The observed HO_2/OH ratios were used for analysis only when HO_2 and OH measurements were made at least once and twice, respectively, in the pertinent 10-min period, and the averaged OH concentrations exceeded 1×10^6 and 5×10^5 radicals cm^{-3} in the daylight period (04:00–19:00 UTC) and nighttime (other period), respectively.

Very recently, Fuchs et al. (2011) showed that HO_2 measurements by the FZJ instrument had large sensitivities toward organic peroxy radicals, such as those formed from isoprene, olefins, including methacrolein (MACR) and methyl vinyl ketone (MVK), and aromatic compounds. The MPI instrument has a similar degree of interference (Dillon, 2011) and it is possible that it occurs also with the FRCGC instrument, which used the same conversion process of HO_2 to OH (reaction with added NO) and achieved high conversion efficiencies, similar to those obtained by the FZJ instrument. However, this has not yet been fully characterized with the MPI and FRCGC instruments. In this paper, the HO_2 levels observed by FZJ are compared with the modeled values, taking into account the sensitivity toward speciated RO_2 radicals. In this paper HO_2(*) represents the sum of the modeled HO_2 and the interference from modeled RO_2 weighted by the relative detection sensitivities. More details will be described in Sect. 3.

The OH reactivity was measured with an instrument using a pump-and-probe method developed by Tokyo Metropolitan University (Sadanaga et al., 2005; Yoshino et al., 2006) by sampling ambient air at similar heights. The uncertainty in the reactivity data during this field campaign was estimated to be 15 %.

Standard instruments recorded humidity, ozone, and meteorological data. The ambient temperature was moderate, peaking at 28 °C on 10 July. On 9 July, ground fog was present until 08:10 UTC and later it was sunny with scattered clouds. It was almost cloud-free on 10 July. Although it was sunny until 14:00 on 11 July, a rainstorm occurred after that. NO and NO_2 were measured using an instrument from Eco Physics (Duernten, Switzerland). CO was measured by a GC-RGD (gas chromatography/reduction gas detector). $J(O^1D)$, $J(NO_2)$, J(HONO), $J(HCHO)_{radical}$, $J(HCHO)_{molecule}$, and $J(H_2O_2)$ were determined with a spectral actinic flux radiometer. See Fig. 3 of Schlosser et al. (2009) and Fig. 2 of Fuchs et al. (2010) for NO_x, O_3, and $J(O^1D)$ values. Briefly, ozone concentrations showed similar daytime peaks (62–65 ppb) for all three days. NO showed morning peaks of about 12, 2, and 5 ppb on the three days (see also Fig. S1). It should be noted that NO reached a level as low as 0.17 ppb during 12:00–16:00 UTC on 10 July (Sunday). HONO was measured by a long path absorption photometer (Heland et al., 2001; Kleffmann et al., 2005). HONO showed a typical diurnal variation with highest concentrations around sunrise (300–600 ppt) and lower concentrations (80–160 ppt) in the early afternoon (12:00–15:00 UTC). Multiple GC systems measured non-methane hydrocarbons and other VOCs at a frequency of 50 min. These included ethane, ethene, acetylene, propane, propene, isobutane, isobutene, but-1-ene, *trans*-butene, isopentane, *n*-pentane, *cis*-2-pentene, *n*-hexane, *n*-heptane, *n*-octane, *n*-decane, benzene, toluene, ethylbenzene, *o*-xylene, *m*-xylene, *p*-xylene, butanal, butanone, isoprene, MACR, MVK, propanal, acetone, and acetaldehyde.

Table 1. Instruments measuring OH and HO_2 during the ambient measurement period of the HO_xComp campaign.

	OH accuracy (1σ) (%)	OH LOD ($S/N=2$) (10^5 cm^{-3})	Δt (s)	HO_2 accuracy (1σ) (%)*	HO_2 LOD ($S/N=2$) (pptv)	Δt (s)
DWD_CIMS	19	4.5	8			
FRCGC_LIF	20	5.3	73	24	0.22	73
MPI_LIF	16	11	5	16	0.68	5
FZJ_LIF	10	4.9	137	10	0.86	30

* HO_2 accuracies do not include possible systematic errors due to interference by RO_2.

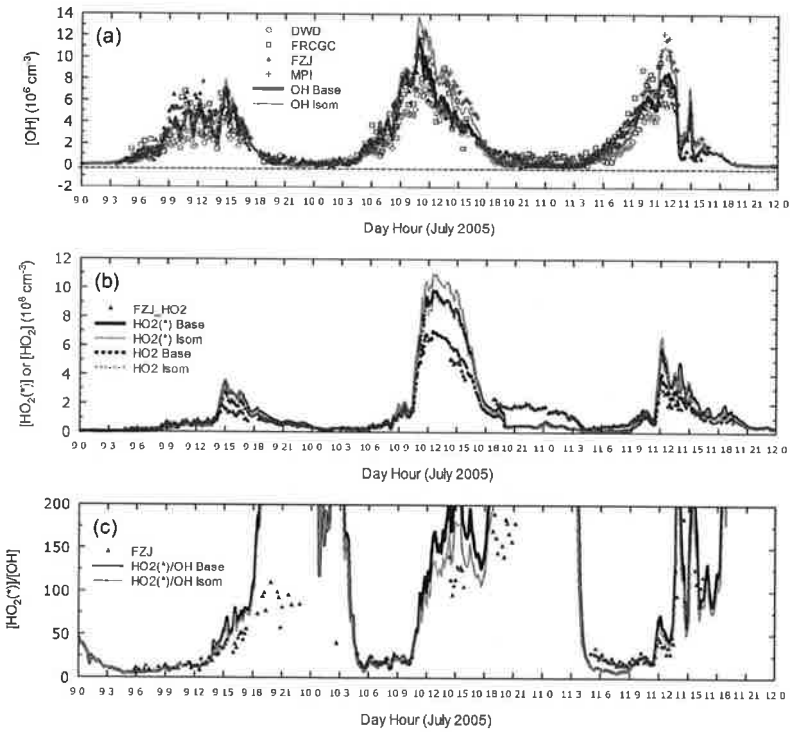

Fig. 1. Comparisons of observed and modeled **(a)** OH and **(b)** HO_2(*) concentrations, and **(c)** HO_2(*)/OH ratios. The results from the Base and Isom runs are shown.

Isoprene concentrations showed diurnal variations, with daytime maxima. The average midday (09:00–15:00 UTC) isoprene concentrations were 0.45, 0.71, and 1.16 ppb for the three days (see Fig. S1). A maximum isoprene concentration (2.4 ppb) was recorded at 15:21 UTC on 11 July. HCHO was measured using a Hantzsch AL-4001 monitor (Aero-Laser, Garmisch-Partenkirchen, Germany). Typical midday concentrations were 2–3 ppb. Measurement uncertainties of the trace gases are listed in Table S2. The sunrise, local noon, and sunset occurred at 03:34–03:36, 11:39, and 19:43–19:45 UTC, respectively.

3 Model simulations

The photochemical box model we used is based on the regional atmospheric chemistry mechanism (RACM) designed by Stockwell et al. (1997), but the isoprene chemistry is revised for the Base run (Table 2), as shown in Table S1 (except A57–74 reactions). The Base mechanism adopts the isoprene chemistry from MCM ver. 3.1 (http://mcm.leeds.ac.uk/MCM/) and is further updated with the recently discovered epoxide formation mechanism (Paulot et al., 2009), while isomerization of isoprene peroxy radicals is not taken into account. Kinetic parameters and product yields of the

mechanism were mainly taken from Pöschl et al. (2000), Peeters and Müller (2010), Stavrakou et al. (2010), Taraborrelli et al. (2009), and Paulot et al. (2009). The advantages over the original RACM are that MVK is taken into account as a separate species and that a third product (e.g., HALD5152) represents unmeasured secondary species, even if MACR and MVK are both constrained to observations. In the Isom run (Table 2), isomerization of isoprene peroxy radicals (at rates proposed by Peeters and Müller, 2010) and some modified reactions are taken into account by introducing A57–74 reactions. This allowed formation of unsaturated hydroperoxy aldehydes, HPALD1 and HPALD2, whose photolysis frequencies were assumed to depend on the solar zenith angle, similar to the dependence of MACR, and the maximum value (with overhead sun) was assumed to be $5 \times 10^{-4}\,s^{-1}$, as suggested by Peeters and Müller (2010). The photolysis of HPALD1 and HPALD2 gave peroxy-acid-aldehydes, PACALD1 and PACALD2, in addition to OH and HO_2. The photolysis of PACALD1 and 2 was assumed to be twice faster than that of HPALD1 and 2 (Peeters and Müller, 2010).

For all runs, several kinetic parameters and yields in the original RACM were also revised: the rate coefficients of the $O(^1D) + N_2$ and $OH + NO_2 + M$ reactions were taken from Ravishankara et al. (2002) and MCM ver. 3.1, respectively. OH production from acylperoxy + HO_2 radical reactions, recently proved by Dillon and Crowley (2008), was taken into account. The rate coefficients of the $RO_2 + NO$ and $RO_2 + HO_2$ reactions (except peroxy radicals from methane, ethane and ethene and acylperoxy radicals) were taken from MCM ver. 3.1. The dry deposition velocities of H_2O_2, HNO_3, carbonyl species, peroxyacyl nitrates, nitrates, and organic peroxides were assumed to be 1.1, 2.0, 0.5, 0.2, 1.1, and 0.55 $cm\,s^{-1}$, respectively (Brasseur et al., 1998; Zhang et al., 2003). The change in the boundary layer height (300 m during nighttime, linear increase to 1300 m from 06:00 to 14:00 UTC, constant at 1300 m until 19:50 UTC, and an immediate drop to 300 m at 19:50 UTC) was taken into account in representing the deposition loss flux.

All of the ancillary observations were averaged or interpolated with a time resolution of 10 min and used as model constraints. Data gaps were basically filled by linear interpolation. Photolysis frequencies other than those directly measured were estimated. In detail, clear-sky values were first calculated by using parameterized equations as functions of the solar zenith angle and then they were multiplied by a "cloudiness factor", defined as the ratio of measured $J(NO_2)$ to calculated clear-sky $J(NO_2)$. A multiplication factor of 1.05 was used to account for upwelling fractions of J values.

The diurnal variation of the air composition at the measurement site was modeled for each day separately in a two-step approach assuming that isoprene was emitted only by the nearby forest and photochemically processed shortly (12 min, see below) before the advected air arrived at the measurement site.

In the first step, the model was constrained to the observations, but with isoprene, MACR and MVK set to zero. The time 00:00 UTC was regarded as the initial time on each day, and integration over 24 h was conducted by 10-min binning of the data. The integration was conducted five times in series to stabilize the concentrations of unconstrained species (e.g., unmeasured carbonyl and peroxide species). Thus, after a spin-up time of four days, the last 24 h determined the diurnal variation of the modeled species in the absence of isoprene chemistry. In the second step, the air composition at each time of the day was recalculated in a follow-up run of 12 min duration. Here, the calculated output from modeling step 1 was used for initialization and observations including the measured concentrations of isoprene, MACR and MVK were used as constraints. As a result, step 2 simulates HO_x concentrations after the air has been exposed to fresh isoprene emissions for a short oxidation time of 12 min only. This special treatment was employed because MACR and MVK concentrations, two major photochemical products of isoprene, were significantly overestimated (by factors of ca. 2.5) when isoprene concentrations were constrained to observations for the full five days (for this test MACR and MVK were unconstrained), indicating the possibility that isoprene reaction is too short for the secondary products to reach daytime quasi-steady-state concentration levels. In the full calculation, where MACR and MVK concentrations are constrained to observations, this special treatment is effective only for the determination of concentrations of other secondary products (e.g., HALD5152 in the Base run). Our two-step approach yields modeled OH concentrations which are only 3 % larger than in the case where isoprene was continuously taken into account for five model days (one-step approach), whereas the modeled HO_2 concentrations and the OH reactivity are 6 % and 10 % smaller, respectively.

The 12-min period was optimized in pre-runs for individual chemical mechanisms (those used in the Base and Isom runs), where the constraint of the MACR and MVK concentrations were removed, such that the observed sum concentrations of MACR and MVK are reproduced (see Fig. S2): with isoprene oxidation durations of 10, 12, and 20 min, calculated MACR + MVK concentrations varied from 97 % to 115 % and 183 % of observations as midday (09:00–15:00 UTC) averages over the three days for the chemical mechanism of the Base run. The same values were 87 %, 104 %, and 168 % for the chemical mechanism of the Isom run. The 12-min period is in rough agreement with the traveling time for the air mass required to pass over the adjacent forest area (fetch is about 1–2 km), present in the upwind direction and deemed as the major source of isoprene. The wind speed ($2.6 \pm 0.7\,m\,s^{-1}$) and direction (355 ± 17 degrees) were fairly stable for the midday (09:00–15:00 UTC) periods of the three days. Outside the forest, the air had passed for more than 20 km over agricultural land (growing mostly wheat, corn, and sugar beets), outskirts of Jülich and a few small villages, where isoprene emissions would be

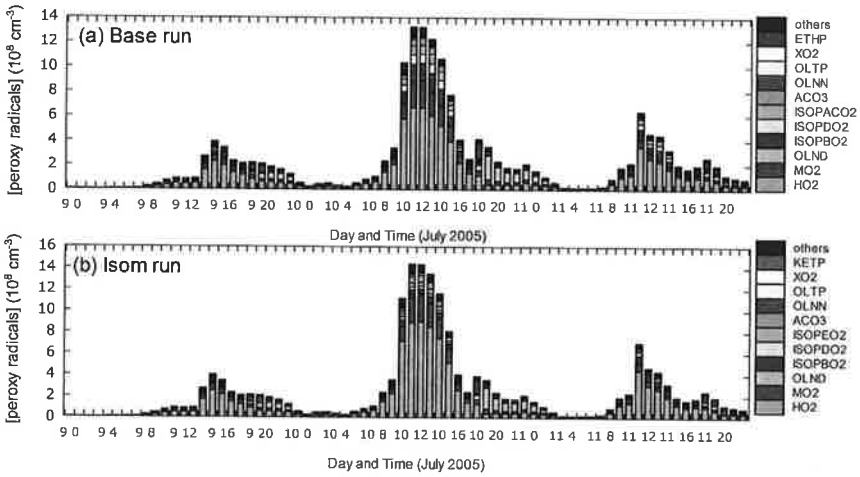

Fig. 2. Breakdown of peroxy radicals (HO_2 and RO_2) in the Base and Isom runs. MO2, OLND, OLNN, ACO3, OLTP, ETHP, KETP, and XO2 stand for methyl peroxy radical, NO_3-alkene adduct (reacting via decomposition), NO_3-alkene adduct (reacting to form HO_2), saturated acylperoxy radicals, peroxy radicals from OLT (terminal olefins), peroxy radicals from ethane, peroxy radicals from ketones, and parameterized peroxy radicals accounting for additional NO to NO_2 conversions, respectively.

Table 2. Descriptions of model runs.

Name	Isomerization of isoprene peroxy radicals; photolysis of HPALDs	NMHC added to explain observed OH reactivity	Additional HO_2 loss
Base run	NO	NO	NO
Isom run	YES	NO	NO
Base_a (HC8)	NO	HC8	NO
Base_b (XYL)	NO	XYL	NO
Base_c (API)	NO	API	NO
Base_d (OLI)	NO	OLI	NO
Base_e (mix)	NO	32 % from HC8, XYL, and API and 4 % from OLI	NO
Isom_a (HC8)	YES	HC8	NO
Base_e(mix)_HO_2_loss	NO	32 % from HC8, XYL, and API and 4 % from OLI	$HO_2 \rightarrow 0.75$ OH ($0.2\,s^{-1}$)

smaller. Komenda et al. (2003) and Ammann et al. (2004) also suggested the importance of local emission for isoprene on the same campus.

During nine 10-min periods, when valid NO measurements were not available or one standard deviation (calculated on the basis of raw data at ca. 100-s frequencies) exceeded the averages, the model results were not used in further analyses.

For the reconstruction of HO_2(*), the following RO_2 radicals were taken into account with relative sensitivities specified in parentheses (Fuchs et al., 2011; Lu et al., 2012): ETEP (0.85), OLTP (0.95), OLIP (0.95), isoprene peroxy radicals (ISOPBO2, ISOPDO2, ISOPACO2, and ISOPEO2) (0.79), TOLP (0.86), XYLP (0.86), CSLP (0.86), and MACP (0.58). ETEP, OLTP, OLIP, TOLP, XYLP, CSLP, and MACP are peroxy radicals formed from ethene, terminal olefins (OLT), internal olefins (OLI), toluene and less reactive aromatics, xylene and more reactive aromatics (XYL), hydroxyl substituted aromatics, and MACR, respectively.

Monte-Carlo simulations for the Base run, where the uncertainty ranges of the reaction rate coefficients and of ancillary observations were taken into account (Tables S2 and S3; the values were taken from Sander et al. (2003) and Kanaya et al. (2007a) or determined from typical instrumental uncertainties and temporal variations), yielded total uncertainties (1σ) for the OH and HO_2(*) concentrations and HO_2(*)/OH

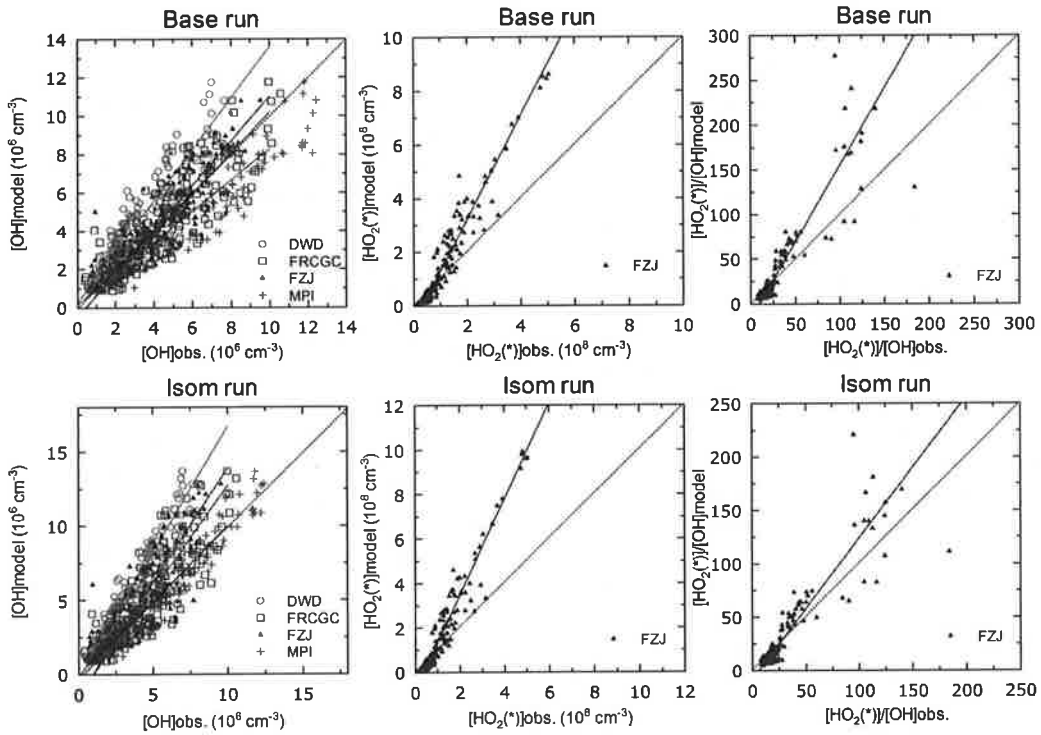

Fig. 3. Scatterplots between observed OH and $HO_2(*)$ concentrations and $HO_2(*)$/OH ratios, and those modeled in the Base run (upper panels) and in the Isom run (lower panels). Linear regression lines are shown by colored solid lines and one-to-one lines are given as black dotted lines.

ratios of 28 %, 32 %, and 19 % for the noontime of 9 July and 19 %, 16 %, and 19 % for the noontime of 10 July, respectively. Monte-Carlo simulations for the Isom run yielded total uncertainties (1σ) for the OH and $HO_2(*)$ concentrations and $HO_2(*)$/OH ratios of 18 %, 16 %, and 16 % for the noontime of 10 July. The rate coefficient of the OH + NO_2 + M reaction newly determined by Mollner et al. (2010) with reduced uncertainty, 22 % slower than that used in the model runs in this study, is still within the uncertainty (a factor of 1.3, Table S3) taken into account in the Monte-Carlo analysis. A sensitivity model run employing the new rate yielded about 13 % larger OH than the original run.

4 Results and discussion

4.1 Comparisons with Base run

Figure 1a and b show time series of observed and modeled OH and $HO_2(*)$ concentrations. In the Base run, the features of the temporal variations of OH are basically captured quite well by the model simulations. The order of the general magnitudes of the relationships is MPI > Base run > FRCGC > FZJ > DWD for OH. For $HO_2(*)$, the Base run gives higher values than FZJ in the daytime after 12:00 UTC, while agreement is better during 06:00–12:00 UTC. The relationship for the $HO_2(*)$/OH ratio (Fig. 1c) is similar; while the observed ratios in the morning (06:00–12:00 UTC) are well reproduced by the model (except on 11 July, after attachment of the RO_x converter (see Fuchs et al. (2010) for details)), the ratios in the afternoon (12:00–18:00 UTC) are often overestimated. In Figure 1b, original HO_2 concentrations in the Base model run, without taking into account the RO_2 interference, are also shown to indicate the degrees of influence of RO_2 on the HO_2 observations. Figure 2a shows the breakdown of peroxy radicals (RO_2 and HO_2) in the Base run. The major organic peroxy radicals are MO2 (CH_3O_2), isoprene peroxy radicals (ISOPBO2 + ISOPDO2 + ISOPACO2), saturated acylperoxy radicals (ACO3), and those from terminal olefins (OLTP) in the daytime. The RO_2/HO_2 ratio ranged from 0.64 to 1.05 in the daytime and this resulted in the $HO_2(*)/HO_2$ ratio ranging from 1.16 to 1.61 (Fig. 1b).

Figure 3 (upper panels) shows scatterplots for observed and modeled OH and $HO_2(*)$ concentrations and $HO_2(*)$/OH ratios in the daytime period (06:00–18:00 UTC). Table 3 includes linear-regression parameters for these plots. All of the OH concentrations observed by the four instruments are fairly well reproduced by the Base model run (slopes

(model/observation) range from 0.81 to 1.33), with high R^2 values (0.72–0.93). The intercepts for OH range from -5.0×10^5 cm^{-3} to 2.5×10^5 cm^{-3}. They are considered to be negligible when the uncertainties of the model calculation and observations are taken into account. For HO_2(*) and HO_2(*)/OH ratio, the model overestimated the measurements by 93 % and 72 %, respectively, while the R^2 values are high (0.93 and 0.79). In Table 3, linear regression parameters for HO_2 observations with modeled HO_2 (not including RO_2 interference) are also listed for comparison. The slopes (model/observation) for HO_2_FRCGC and HO_2_MPI are 1.11 and 0.81. If a potential interference from RO_2, although not quantified yet, is added to the model, the slopes will become significantly larger than unity similar to the FZJ case. The regression line for the HO_2/OH ratios with respect to the MPI data has a significant negative intercept value (−54) in comparison with the Base run (Table 3). The RO_2 interference with the MPI instrument in the HO_2 measurements might be related to this.

The NO/NO_2 cycle is linked to the HO_2/OH cycle. When the NO_2 concentrations were unconstrained but calculated in the model (i.e., photochemical equilibrium), the daytime NO_2 concentrations on the three days were lowered by 24–28 % from the observed levels. Simultaneously the OH and HO_2(*) levels increased by 3–30 % and 2–27 %, respectively, and the HO_2(*)/OH ratio was almost unchanged (1 % reduction). This does not bring the model results into agreement with the observations. Removing the NO constraint instead increased the daytime NO and OH concentrations by 34–43 % and 0–24 %, respectively, and decreased HO_2(*) by 5–31 %, resulting in a reduction in the modeled HO_2(*)/OH ratio by 23–29 %. In this case, the disagreement in the observed and modeled HO_2(*) levels and the HO_2(*)/OH ratio is partially diminished. However, it is not likely that such a large bias is present for the NO observations rather than NO_2, considering that NO undergoes direct reaction with O_3 in the chemiluminescence instrument while NO_2 measurements require an additional step of photolytic conversion to NO. Therefore the overestimation of the HO_2(*)/OH by the model cannot be fully explained by the uncertainties in the NO_x measurements used as constraints, while the deviation of the NO/NO_2 ratio from photochemical equilibrium needs further investigation.

The result of our model-measurement comparison is surprisingly different from the findings of other campaigns which reported strong underprediction of observed OH levels at high VOC and low NO_x conditions. Here, we find that the Base model reproduces the measured OH at HO_xComp fairly well to within 33 % over a range of 0.3–2 ppb isoprene and at NO mixing ratios as low as 0.1 ppb. The different conclusion cannot be attributed to our model assumption of a short time period in which the isoprene chemistry is effective, because OH from our two-step model approach differs by only 3 % from the result of the one-step approach (with isoprene being effective for five days; see Sect. 3). In fact, Elshorbany et al. (2012) applied the one-step approach to simulate the diurnal OH profile at HO_xComp on 10 July using the MCM v3.2 chemical mechanism. They reached the same conclusion, namely that the modeled OH agrees with the observations by all four measurement instruments within 30 %. Interestingly, under conditions with similar mixing ratios of isoprene and NO, observed OH was underpredicted by a box model by up to a factor of 8 in PRD (Hofzumahaus et al., 2009; Lu et al., 2012). In those studies, the mean OH reactivity and OH concentration were both a factor of two larger than at HO_xComp, resulting in four times larger OH turnover rates during noontime. At even lower NO (<0.1 ppb) and in the presence of a few ppb isoprene, measured-to-modeled OH ratios reached even values up to ten in the rain forest in Suriname (Lelieveld et al., 2008) and Borneo (Whalley et al., 2011; Stone et al., 2011). In order to explain these large model-measurement discrepancies, unknown radical recycling reactions were postulated as additional OH source (Lelieveld et al., 2008; Hofzumahaus et al., 2009; Whalley et al., 2011). Apparently, such processes do not seem to play an important role for HO_xComp, or were possibly masked by other effects.

The experimental analysis of the OH budget at HO_xComp by Elshorbany et al. (2012) indicates an unknown OH source in the afternoon of 10 July, when the NO concentration decreased to values below 1 ppb. They estimated the missing OH source to be in the range of 2-4 ppb h^{-1} by comparing the OH loss rate (calculated from the measured OH reactivity and OH concentration) with the known OH production rates from HO_2 recycling, photolysis of ozone and HONO, and ozonolysis of alkenes. The missing OH source seems to contradict the good agreement of our modeled and measured OH. However, we have to consider that HO_2(*) is significantly overpredicted by the model in the afternoon at low NO_x (Fig. 1), causing a corresponding overprediction of the HO_2 to OH recycling in the model. In fact, if we include additional loss processes for HO_2 in order to match the modeled and measured HO_2(*), we also need an additional OH source of about 4.7 ppb h^{-1} (for the afternoon of 10 July) to reproduce the observed OH (see details in Sect. 4.3). Thus, the good agreement of the modeled and measured OH for the Base model run apparently results from canceling of systematic errors in the modeled OH production and destruction terms.

The degree of agreement for OH between the FRCGC results and the Base model run is better than in past studies using the same instruments and the standard RACM model calculations. At Rishiri Island in 2003, the calculated/observed ratio for OH was 1.35, with an R^2 value of 0.76 (Kanaya et al., 2007a). In central Tokyo, the calculated/observed ratio for OH was 0.86 in the summer, with an R^2 value of 0.41 (Kanaya et al., 2007b).

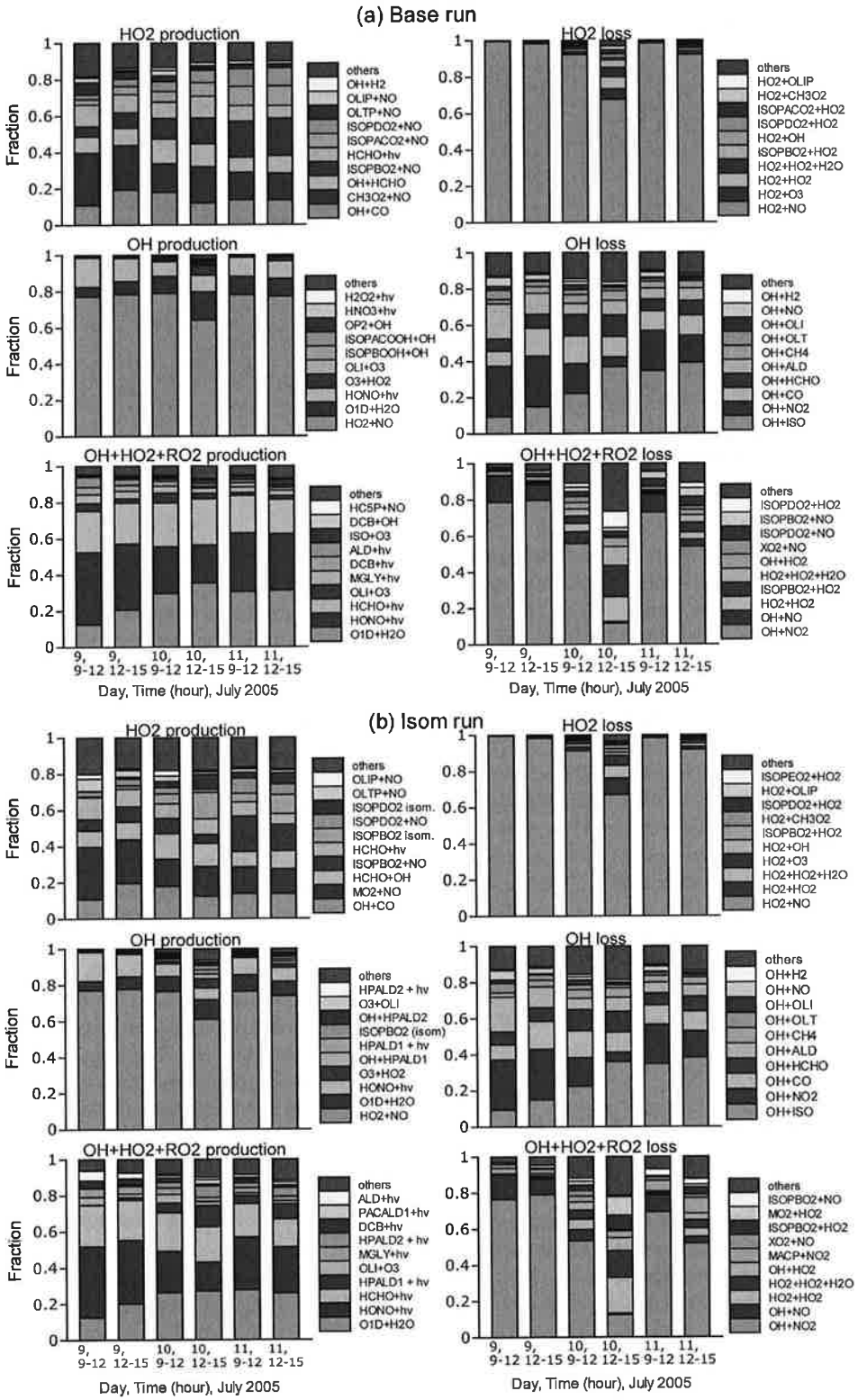

Fig. 4. Breakdown of production and loss processes of OH, HO_2, and radical group ($OH + HO_2 + RO_2$) in the Base and Isom runs.

Table 3. Linear-regression parameters for daytime (defined as 06:00–18:00 UTC). Slopes larger than unity indicate model overestimation. Intercepts are for the y-axis for model values.

	Base			Isom			Base_e(mix)			Isom_a(HC8)			Base_e(mix)_HO_2 loss		
	slope	intercept	R^2	slope	intercept	R^2	slope	intercept	R^2	slope	intercept	R^2	slope	intercept	R^2
OH_DWD	1.33	2.5×10^5	0.86	1.70	-2.8×10^5	0.93	1.32	7.9×10^5	0.69	0.99	4.6×10^5	0.78			
OH_FRCGC	1.06	-4.4×10^5	0.72	1.42	-1.5×10^6	0.70	1.02	2.3×10^5	0.66	0.76	7.4×10^4	0.70			
OH_FZJ	1.15	-5.0×10^5	0.79	1.54	-1.5×10^6	0.72	1.15	9.1×10^2	0.73	0.85	-1.1×10^5	0.80	0.96	2.7×10^5	0.81
OH_MPI	0.81	1.7×10^5	0.87	1.04	-3.5×10^5	0.94	0.79	7.2×10^5	0.71	0.60	3.7×10^5	0.80			
HO_2 (*)_FZJ[a]	1.93	-6.5×10^7	0.93	2.15	-8.3×10^7	0.93	2.49	-4.8×10^7	0.88	1.73	-5.3×10^7	0.92	1.29	-2.1×10^7	0.93
HO_2 (*)/OH_FZJ[a]	1.72	-1.6×10^1	0.79	1.32	−7.9	0.80	2.12	-1.5×10^1	0.83	1.68	−8.3	0.83	0.88	3.1	0.81
HO_2_FRCGC[b]	1.11	-1.8×10^7	0.97	1.52	-4.5×10^7	0.98	1.32	1.7×10^7	0.93	1.18	-1.8×10^7	0.97			
HO_2_FZJ[b]	1.33	-3.8×10^7	0.91	1.81	-7.5×10^7	0.92	1.85	-2.9×10^7	0.85	1.51	-4.8×10^7	0.92	0.51	1.6×10^7	0.64
HO_2_MPI[b]	0.82	-6.3×10^7	0.95	1.13	-1.1×10^8	0.95	0.97	-2.9×10^7	0.94	0.87	-6.6×10^7	0.95			
HO_2/OH_FRCGC[b]	1.15	−5.3	0.90	1.12	−4.9	0.90	1.57	−6.1	0.90	1.55	−7.2	0.89			
HO_2/OH_FZJ[b]	1.14	−7.7	0.78	1.11	−7.2	0.78	1.52	−7.3	0.82	1.47	−7.6	0.81	0.25	1.0×10^1	0.66
HO_2/OH_MPI[b]	1.72	-5.4×10^1	0.86	1.69	-5.3×10^1	0.86	2.38	-7.2×10^1	0.88	2.36	-7.4×10^1	0.87			
OH reactivity mean bias (obs − model)	1.65			1.67			−0.29			−0.26			−0.17		

Units for the intercept and OH reactivity are cm^{-3} and s^{-1}, respectively.
[a] HO_2(*) indicates comparisons with modeled $HO_2 + RO_2$ artifacts. See text for details.
[b] Comparisons were made using modeled HO_2 (without taking into account RO_2 interference).

Figure 4a shows the breakdown of the production and loss processes of HO_2, OH and the radical group ($OH + HO_2 + RO_2$) for the Base run. They are separately shown as 3-h averages (09:00–12:00 and 12:00–15:00 UTC) on the three days. In the Base run, HO_2 production is contributed mainly by the isoprene peroxy radical (ISOPBO2, ISOPDO2, ISOPACO2) + NO reactions (11–41 %), OH + CO (11–18 %), CH_3O_2 + NO (15–29 %), HCHO + OH (9–14 %), and HCHO + $h\nu$ (9–12 %). HO_2 loss is dominated by reaction with NO (>68 %). OH production is largely from the HO_2 + NO reaction (>64 %). OH loss is dominated by reactions with isoprene (9–39 %, especially high in the afternoon), CO (8–15 %), and NO_2 (5–28 %, large in the morning). The major radical initiation sources for the radical group ($OH + HO_2 + RO_2$) are $O(^1D) + H_2O$ (13–35 %), HONO + $h\nu$ (21–40 %), and HCHO + $h\nu$ (19–26 %). Terminal radical loss is mainly from OH + NO_2 (54–80 %), except for the afternoon of 10 July, when reactions of isoprene peroxy radicals with HO_2 and the HO_2 recombination reactions largely contributed (79 %).

4.2 Comparisons with Isom run

Next, we study the effects of the revised isoprene chemistry, postulated by Peeters and Müller (2010) to explain the missing OH source in forest environments. The results for HO_xComp are shown in the same figures as the Base run (Figs. 1–3). The isoprene-chemistry revision increased OH, HO_2, and HO_2(*) concentrations, by 28 %, 38 %, and 13 % on average for daytime (06:00–18:00 UTC), with respect to the Base run results. Averaged HPALD1 and HPALD2 concentrations in the afternoons (12:00–15:00 UTC) of 10 and 11 July, when isoprene concentrations were high, were 124 ppt (HPALD1) and 71 ppt (HPALD2) for the Isom run. The dominant RO_2 radicals (Fig. 2b) are MO2, isoprene peroxy radicals (ISOPBO2 + ISOPDO2 + ISOPEO2), and ACO3, similar to those in the Base run (Fig. 2a). The RO_2/HO_2 ratio for the Isom run was 0.57–0.81 in the daytime, smaller than the Base run (0.64–1.05). Therefore HO_2(*) increased only by 13 % by the isoprene-chemistry revision, while HO_2 increased by 38 %.

The OH concentrations in the Isom run are significantly higher than those derived from the observations by DWD, FRCGC, and FZJ, at least at noon of 10 July, for which the model's uncertainties are calculated on the basis of a Monte-Carlo approach, but they are in reasonable agreement with the MPI observations. Figure 3 and Table 3 show that the results from the Isom run are 42–70 % higher than OH measured by DWD, FRCGC, and FZJ, although they are only 4 % higher than the observations made by MPI. The differences for OH measurements by DWD, FRCGC, and FZJ cannot be explained by the combined 1σ uncertainties of observations and model calculations. The degree of overestimation for HO_2(*) is 115 %, even larger than in the case of the Base run (93 %), while that for the HO_2(*)/OH is 32 %, milder than in the case of the Base run (Table 3). The regression lines for the HO_2/OH ratios with respect to the MPI data has significant negative intercept values (−53) again, suggesting that the isomerization does not influence this.

Figure 4b shows the breakdown of the production and loss processes of HO_2, OH and the radical group ($OH + HO_2 + RO_2$) for the Isom runs. Isomerization of isoprene peroxy radicals and photolysis of HPALD1, HPALD2, PACALD1, and PACALD2 became important for OH production (by up to 9 %), HO_2 production (by up to 27 %), and total radical production (by up to 22 %). The loss processes are not much different from those in the Base run, but the $HO_2 + HO_2$ reaction became more important (35 %

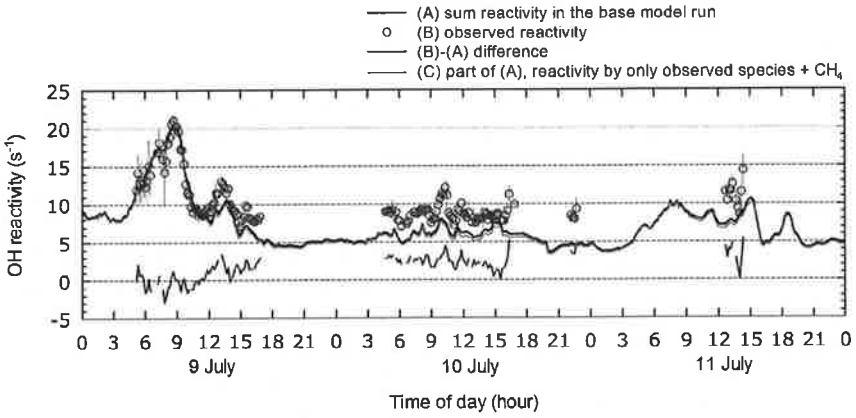

Fig. 5. OH reactivities observed by Tokyo Metropolitan University group (B, blue) compared with the sum of OH reaction rates with respect to all chemical species (A), including those measured and others calculated in the Base run (black). Green (C) shows the fraction of calculated reactivities attributable to reactions with observed species (including methane). The difference between the observed (B) and modeled total (A) reactivities is shown in red; this is used as a basis for calculating amounts of additional hydrocarbon assumed in further model runs.

contribution for the radical loss) because of the larger HO_2 concentrations in the Isom run.

The gross OH production rates in the Isom run in the period 12:00–15:00 UTC on 10 and 11 July (7.9 and 8.0 ppb h^{-1} respectively) were 43 % and 26 % higher than those in the Base run (5.5 and 6.4 ppb h^{-1}, respectively) as a result of additional recycling of OH by isomerization of isoprene peroxy radicals. The total radical ($OH + HO_2 + RO_2$) initiation rates for S1 in the same periods (3.2 and 2.4 ppb h^{-1}, respectively) were 31 % and 22 % higher than those in the Base run (2.4 and 2.0 ppb h^{-1}, respectively).

The implementation of the revised isoprene chemistry (Isom run) introduces an additional OH source which has a value of 2.5 ppb h^{-1} around noon on 10 July. This additional production rate has approximately the magnitude that was missing in the experimental OH budget analysis by Elshorbany et al. (2012). However, it is largely contributed by the increased HO_2-to-OH recycling (based on the increased HO_2 concentrations) in the Isom run that is not supported by the HO_2(*) observations. Therefore the increased OH production in the Isom run will not explain the missing OH source estimated by Elshorbany et al. (2012).

The revised isoprene chemistry (Isom run) improves the agreement between our model result and the OH measurement by MPI. It is interesting to note that it was the same MPI instrument that flew over Suriname (with high isoprene concentrations) that measured OH and HO_2 concentrations higher than those modeled, for which the isomerization mechanism was proposed as an explanation. In case of the other instruments, however, the agreement between modeled and measured OH becomes significantly worse, with model-to-measurement ratios of 1.4–1.7. In addition, the model overprediction of HO_2(*) increases further from a factor of 1.9 to 2.1. Thus, the HO_xComp observations by FZJ, FRCGC and DWD do not support the isomerization of isoprene peroxy radicals at the rates proposed by Peeters and Müller (2010). Our finding from the HO_xComp campaign using observation ensembles is consistent with a recent laboratory study (Crounse et al., 2011) suggesting that the isomerization of isoprene peroxy radicals does take place, but at slower rates. It should also be pointed out that the same FZJ instrument (which seems not to support the isomerization mechanism at HO_xComp) was used in PRD, where additional HO_x recycling was postulated to explain the HO_x observations (Hofzumahaus et al., 2009; Lu et al., 2012).

4.3 Comparisons of OH reactivity and additional model runs considering missing hydrocarbons

In Fig. 5, the OH reactivities observed by the Tokyo Metropolitan University group are compared with the sum of the OH reaction rates with respect to each chemical species, including those measured and others (e.g., unmeasured secondary species) calculated in the Base run. Comparison between (A) and (C) in Fig. 5 indicated that the sum reactivity in the Base model run is mainly contributed by reactions with observed species (including methane), rather than those with unmeasured secondary species calculated in the model. Major reactions contributing to (A) can be found in Fig. 4a. The agreement between the observed (B) and calculated (A) reactivities was very good on the morning of 9 July, when the NO_x concentrations were high, but differences were noticeable in the afternoon, typically 1.6 s^{-1}. Similar disagreements of about 2.5 s^{-1} were found in the morning and afternoon of 10 July. Although the observational data were limited, the magnitude of the difference was also similar in the afternoon of 11 July. The missing reactivity might be

explained by unmeasured biogenic hydrocarbons, because isoprene concentrations were larger on 10 and 11 July, when the missing reactivity was large.

Although some part of the discrepancy may be explained by uncertainties of observations and reaction rate coefficients, here we study several cases where this difference is explained by adding selected types of hydrocarbons (at a 10-min resolution). When reactivity observations were not available, the missing reactivities were estimated as the average before and after the period. The missing reactivities were assumed to be $0\,s^{-1}$ and $3\,s^{-1}$ before 05:00 UTC on 9 July and after 14:30 UTC on 11 July, respectively.

The additional model runs we studied as a variant of the Base run were Base_a(HC8), Base_b(XYL), Base_c(API), Base_d(OLI), and Base_e(mix), where the missing reactivity was explained by additional HC8 (reactive alkanes with OH rate constants greater than $6.8 \times 10^{-12} cm^3 s^{-1}$ for case Base_a(HC8)), XYL (xylene and more reactive aromatics for case Base_b(XYL)), API (pinenes for case Base_c(API)), OLI (internal olefins for case Base_d(OLI)), and their mixtures (32 % each from HC8, XYL, and API, and 4 % from OLI for case Base_e(mix)), respectively (Table 2). The contributions from different types of hydrocarbons in the Base_e(mix) run were only determined arbitrarily. The Isom run was modified in that the missing OH reactivity was explained by additional HC8 (called the Isom_a(HC8) run). For this model run, the missing reactivity was recalculated as the difference between observation (when available) and the sum of the reactivities in the Isom model run; this was essentially the same as the results shown in Fig. 5.

In all cases except HC8 addition, not only the added hydrocarbon but also its secondary species non-negligibly contributed to the increase in the reactivity. The added amounts of hydrocarbons were adjusted such that the missing OH reactivities were filled up to within ±6 %. The mean differences in the reactivity (observation - model), about $1.7\,s^{-1}$ in the Base and Isom runs, became about $-0.3\,s^{-1}$ in the Base_e(mix) and Isom_a(HC8) runs (Table 3). The daytime averages of the hydrocarbon concentrations assumed in the model runs were 9.4 ppb of HC8 (in the Base_a(HC8) run), 2.1 ppb of XYL (in the Base_b(XYL) run), 1.7 ppb of API (in the Base_c(API) run), and 1.4 ppb of OLI (in the Base_d(OLI) run). In the Base_e(mix) run, the daytime averages were 3.1 ppb, 0.74 ppb, 0.54 ppb, and 0.13 ppb for HC8, XYL, API, and OLI, respectively. These concentrations are basically much larger than those assumed in the Base run (0.59 ppb of HC8, 0.10 ppb of XYL, 0.081 ppb of OLI, and 0 ppb of API). It is not very likely that a single class of unmeasured hydrocarbons is present at such high concentrations; however, the possibility of the presence of multiple classes of hydrocarbons at smaller concentrations (e.g., Base_e(mix) run) would be higher. For example, monoterpenes have previously been detected at levels of 0.1–0.5 ppb in the forest near the HO_xComp measurement site (Spirig et al., 2005), but were not measured during HO_xComp.

Figure 6a and b show that the addition of HC8 (Base_a(HC8)) reduced OH and HO_2(*) concentrations, but the other runs adding a single class of hydrocarbons to the Base case, especially when adding XYL and OLI, resulted in effective radical-chain amplification, and thus higher HO_x concentrations. In the Base_b(XYL) run, secondary species such as methyl glyoxal (MGLY) and dicarbonyls (DCB) became important, whose photolysis produced radicals effectively. In the Base_d(OLI) run, ozonolysis of added olefins also contributed to the amplification. The Isom_a(HC8) run effectively impeded the radical amplification and brought the OH levels back to the levels of observations by DWD/FRCGC/FZJ (Fig. 6d) but the reduction in the HO_2(*) levels was not enough to match observations by FZJ (Fig. 6e).

Table 3 summarizes the bivariate regression parameters for the Base_e(mix) and Isom_a(HC8) runs. For the Base_e(mix) run, the slope for OH was almost unchanged from those with the Base run, but the discrepancy of HO_2(*) and HO_2(*)/OH ratio with FZJ observations even increased from 93 % to 149 % and from 72 % to 112 %, respectively (see also Fig. 6c for the HO_2(*)/OH ratio). The Base_e(mix) run normally had lower R^2 values than those of the Base run. The Isom_a(HC8) run resulted in slopes (model/observation) nearer to unity for OH levels from DWD (0.99), FRCGC (0.76), and FZJ (0.85), than those obtained for the Isom run ($\geq$1.42). The HO_2(*) discrepancy in the Isom run (149 %) was reduced to 73 % in the Isom_a(HC8) run, but the overestimation of the HO_2(*)/OH ratio was increased from 32 % (Isom run) to 68 % (Isom_a(HC8)) (see also Fig. 6f). Addition of HC8 at large amounts explaining the missing OH reactivity was the only scenario in which the ensemble of OH observations was reproduced with the chemical mechanism including the isomerization. This scenario is not likely because the missing reactivity was small on 9 July, when the influence from anthropogenic hydrocarbons was strong, but was large on 10 and 11 July, when biogenic hydrocarbons were relatively important. In summary, isomerization of isoprene peroxy radicals at the rates proposed by Peeters and Müller (2010) would be unlikely, even when additional hydrocarbons explaining the missing OH reactivities are taken into account.

For the Base_e(mix) run, the large deviations of the slopes from unity for HO_2(*) strongly requires more loss processes for HO_2 (or interfering RO_2) to explain the observations. We tried re-modifications of the Base_e(mix) run by including hypothetical HO_2-loss processes, such that all of the modeled OH, HO_2(*), and HO_2(*)/OH ratios reproduce observations simultaneously. In the run called Base_e(mix)_HO_2_loss, we found that an additional reaction, $HO_2 \rightarrow 0.75$ OH, at a constant rate of $0.2\,s^{-1}$ (Tables 2 and 3) could bring OH, HO_2(*), and the HO_2(*)/OH ratio into agreement with the FZJ observations (Fig. 7); the slopes of the regression lines were 0.96, 1.29, and 0.88, respectively, with high R^2 values, 0.81–0.93 (Table 3). This additional process might be explained

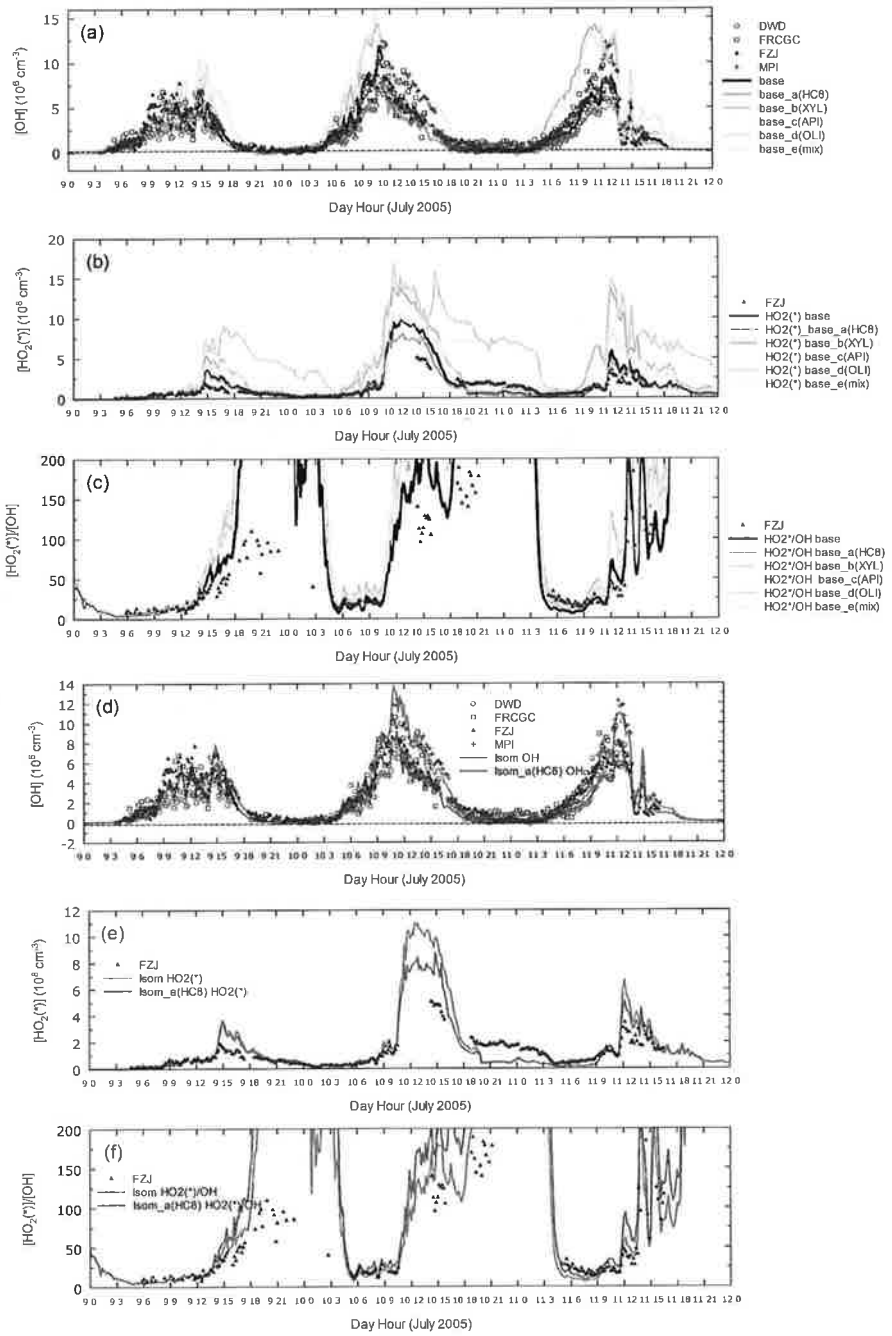

Fig. 6. Comparisons of observed and modeled **(a)** OH and **(b)** HO_2(*) concentrations, and (c) HO_2(*)/OH ratios. The results from the Base run and its variants (Base_a(HC8), Base_b(XYL), Base_c(API), Base_d(OLI), and Base_e(mix)) are shown; **(d)**, **(e)**, and **(f)** are the same as **(a–c)**, but showing the results from the Isom and Isom_a(HC8) runs.

by combination of two processes, $HO_2 \rightarrow$ OH at a constant rate of 0.15 s^{-1} and $HO_2 \rightarrow$ no products at a constant rate of 0.05 s^{-1}. The rate of HO_2-to-OH conversion (0.15 s^{-1}) corresponds to an equivalent NO of 800 ppt. This is much smaller than the 1–7 ppb of equivalent NO required to bring afternoon OH and HO_2(*) levels into agreement with observations in PRD (model M2 in Lu et al., 2012). However, it is hard to suggest any potential processes that could explain

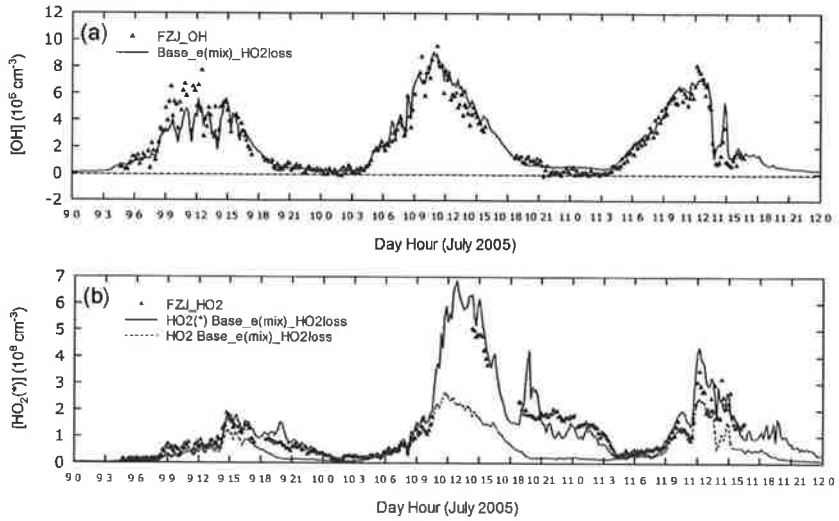

Fig. 7. Time series of observed OH and HO_2 by FZJ instrument, and modeled OH and HO_2(*) in the Base_e(mix)_HO_2_loss run. Modeled HO_2 is also shown for reference.

this additional conversion. The rates of HO_2 loss with no product (0.05 s^{-1}) are also significant, but might be partially explained by heterogeneous loss of HO_2 on aerosol surfaces, whose rates at upper limits have been estimated to be 0.1 s^{-1} for PRD (Lu et al., 2012) and 0.04 s^{-1} for Tokyo (Kanaya et al., 2007b), using a high uptake coefficient ($\gamma \geq 0.5$).

From the budget analysis of the radicals in the Base_e(mix)_HO_2_loss run (Fig. S3), sometimes up to several tens of percents of HO_2 loss, OH production, and radical loss rates need to be explained by the hypothetical HO_2 reactions. Additional OH reproduction at a rate as high as 4.7 ppb h^{-1} is required for the period 12:00–15:00 UTC on 10 July. One reason for this is that the OH production from the HO_2 + NO reaction was slowed in comparison to the Base run (because HO_2 was lowered to reproduce observed HO_2(*) in this run), requiring another OH producing pathway. Another reason is that the OH reactivity in this run, in agreement with observations, is also higher than that in the Base run, requiring more OH production to maintain the OH concentration at the steady state. It should be noted again that such additional OH production is not likely explained by the isomerization mechanism of the isoprene peroxy radicals that leads to the simultaneous production of HO_2 and thus contradicts the additional HO_2 loss required here. Clearly, more studies are needed to explain these discrepancies. Also, RO_2 interference should be quantitatively studied with the FRCGC and MPI instruments.

4.4 Behavior on the morning of 9 July: model's underestimation of HO_2(*) at high NO

Because of the good agreement between observed and simulated OH reactivities and the low isoprene concentrations, the morning of 9 July was deemed to be an ideal period, where all model results tended to converge. Here, the observation ranges are compared to the full range from the model ensemble runs mentioned above (except runs with hypothetical HO_2-loss processes) and to the uncertainty range of the Base run (Fig. 8). The observed OH concentrations from all groups usually fall within the full range of the model ensemble runs and within the uncertainty range of the Base run, except for some high points for FRCGC and FZJ, usually associated with large fluctuations during the 10-min periods (Fig. 8a). The DWD_OH data were slightly lower than the ranges; the observational accuracy could explain these differences. On the other hand, the HO_2(*) concentrations and the HO_2(*)/OH ratios from FZJ were often higher than those from the model results, especially before 10:00 UTC (Fig. 8b and c). The large model-to-observation discrepancies found for this period would most likely be attributable to the possibility of unknown chemistry. Thus, in the following paragraphs, the possibility of unknown chemistry is discussed.

The morning period on 9 July was associated with relatively high NO_x concentrations. In Fig. 9b, where modeled-to-observed HO_2(*) ratios in the daytime (06:00–18:00 UTC) are plotted against NO concentrations, this underestimation by the model is evident only under the high NO conditions seen on the morning of 9 July. This tendency is opposite to the normal low NO cases, where general features were weak overestimations of HO_2(*) (for FZJ), as

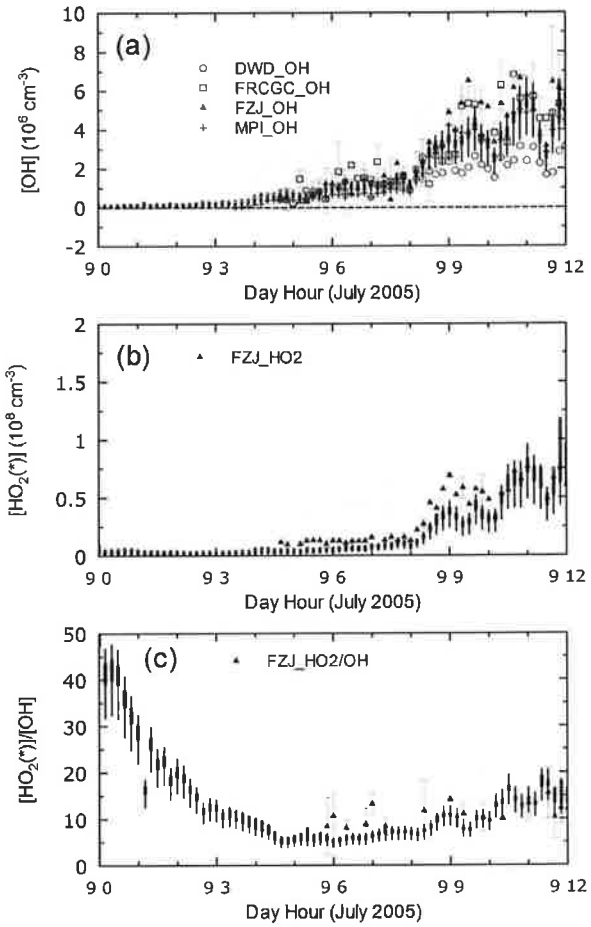

Fig. 8. Comparisons of observed and modeled **(a)** OH and **(b)** $HO_2(*)$ concentrations, and (c) $HO_2(*)$/OH ratios with the full range of model ensemble results (gray bars) and uncertainty range (1σ) of the Base run (black bars) on the morning of 9 July. The colored error bars represent 1σ ranges of observations during 10 min and do not represent systematic uncertainties of the observations.

discussed in the previous sections. The changes in the ratios are smooth against NO. The tendencies of the modeled $HO_2(*)/HO_2$_FRCGC and modeled $HO_2(*)/HO_2$_MPI ratios are also included in Fig. 9b, although the average of the ratios can be biased from unity because of the unknown degrees of RO_2 interference. They also showed decreasing trends with NO, similar to the FZJ case. The RO_2 concentrations become relatively small in comparison to HO_2 in the high NO_x concentration range and thus their interference on the HO_2 measurements cannot explain the tendency. Such a tendency has been discussed before, by Martinez et al. (2003) for Nashville, Ren et al. (2003, 2006) for New York, and Kanaya et al. (2007b) for Tokyo, using a single instrument for each experiment. HO_xComp provided an opportunity to verify this tendency with three instruments being operated simultaneously, for the first time. It is interesting to note that the same tendency is also clear, if the ratio of modeled to observed HO_2 is plotted against NO_2 and NO_x (Fig. 9d), although this was unclear in Tokyo (Kanaya et al., 2007b).

We previously proposed processes that could explain these results (Kanaya et al., 2007b), including 1) HNO_4 reactions, such as reaction with NO producing two HO_2 molecules, and 2) missing HO_x production, with a rate proportional to the NO concentration. An additional HO_xComp model run with hypothetical HO_2 production of strength [NO (cm^{-3})] $\times 5 \times 10^{-5}$ (radicals cm^{-3} s^{-1}) countered the trend of the modeled-to-observed $HO_2(*)$ against NO (not shown). The factor of 5×10^{-5} was larger than that of 2×10^{-5}, which effectively countered the trend in Tokyo (Kanaya et al., 2007b). This trend is very important in the ozone production regime. In Fig. 10, the dependences of the $HO_2(*) + NO$ reaction rates for the midday period (09:00–15:00 UTC) on NO concentrations are shown individually for the values derived from HO_2 observed by the FZJ instrument and for $HO_2(*)$ modeled by the Base run. This reaction normally governs the ozone production. The $HO_2 + NO$ reaction rate coefficient was used in the analysis, although some RO_2 radicals included in $HO_2(*)$ have different coefficients. The modeled rate has a maximum at NO mixing ratios of around 1 ppbv, and then shows saturation with further increases in NO. This saturation corresponds to the "NO_x-saturated" behavior of ozone production at high NO_x. In contrast, the rate using observed HO_2 concentrations monotonously increased with NO, resulting in a permanent NO_x-limited feature. Further studies of the HO_2 behavior at high NO_x conditions in the field and in the laboratory (including chamber studies) are highly recommended.

Figure 9a and c also shows that model/observation ratios for OH are almost flat throughout the NO (and NO_x) concentration ranges for the Base run. This is clearly different from the behavior found in PRD, where the observation/model ratios were >2.5 at NO concentrations of 0.3 ppb (Lu et al., 2012). The different behavior at HO_xComp may be related to the lower isoprene and VOC reactivity or the short time exposure of isoprene to OH. Further studies are also required to explain this difference found for OH.

5 Summary

Daytime OH concentrations in ambient air were observed by multiple instruments for three days of the HO_xComp field campaign held in Jülich, Germany, in July 2005. The concentrations were compared with box-model simulations using different assumptions for isoprene chemistry and for additional hydrocarbons to explain the observed OH reactivity. The agreement in OH concentrations with the Base run was good, suggesting that strong radical production to explain OH in the presence of isoprene at low NO, as proposed for the cases for the measurements in Suriname (Kubistin et

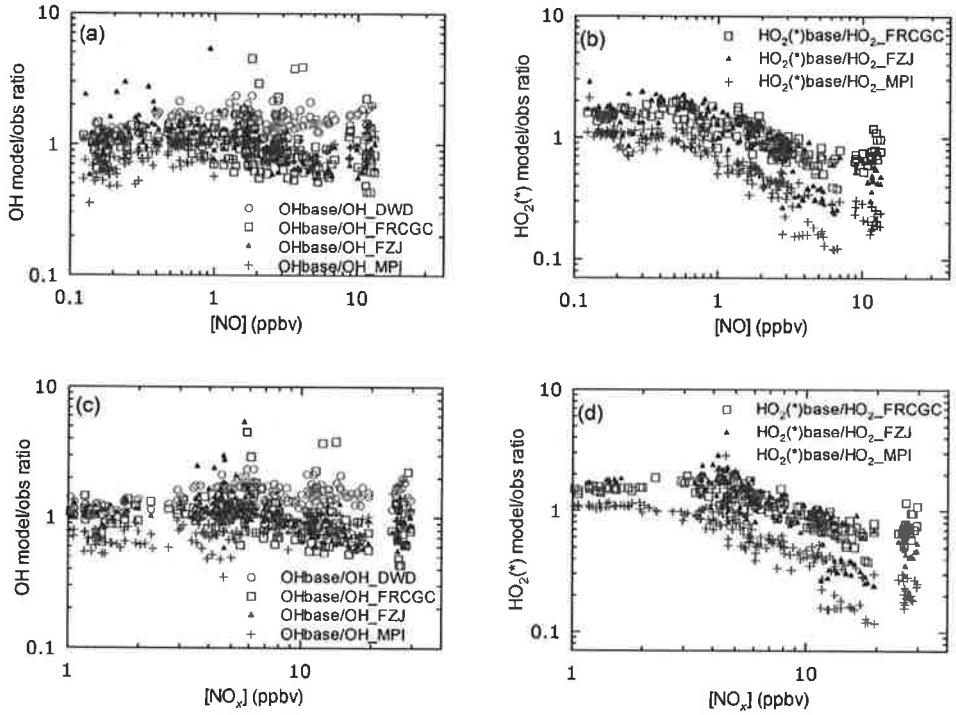

Fig. 9. Model/observation ratios for OH (left) and $HO_2(*)$ (right) as functions of NO and NO_x concentrations for the Base run. Only daytime (06:00–18:00 UTC) data are used.

al., 2010) and PRD (Hofzumahaus et al., 2009; Lu et al., 2012) was not required for HO_xComp. An important difference in the chemical conditions at HO_xComp is the fact that the measurement site experienced fresh isoprene emissions that were only a little photochemically aged. This may be an indication that the unexplained large OH concentrations in Amazonia and PRD were caused by second- or third-generation products from VOC oxidations.

The HO_2 levels measured with the FZJ instrument, for which the degrees of interferences from various RO_2 radicals were known, were compared with the modeled $HO_2(*)$, taking into account the sensitivity toward RO_2. The modeled $HO_2(*)$ levels in the Base run were higher than the observations by a factor 1.9, indicating an overprediction of the HO_2 to OH recycling in the base case model. This and the good model-measurement agreement for OH imply a missing OH source. Modeled OH and $HO_2(*)$ could only be matched to the observations by addition of a strong unknown loss process for $HO_2(*)$ that recycles OH at a high yield.

Introducing isomerization of isoprene peroxy radicals incurred model overprediction of radical concentrations with respect to OH observed by a CIMS instrument and two LIF instruments. The degree of overestimation in OH could be diminished only when reactive alkanes (HC8) were solely introduced to the model to explain the missing fraction of observed OH reactivity. Moreover, the isoprene isomerization

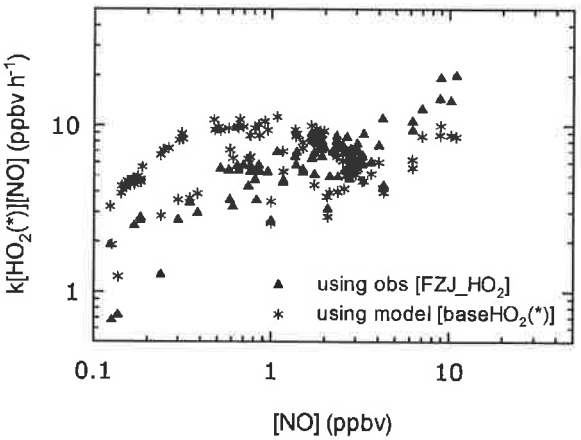

Fig. 10. $HO_2(*) + NO$ reaction rates derived from HO_2 observed by FZJ instrument (blue triangles), and $HO_2(*)$ modeled by the Base run (red stars) plotted as a function of NO. Only midday (09:00–15:00 UTC) data are used.

mechanism could not resolve the strong model overprediction of $HO_2(*)$. The isomerization of isoprene peroxy radicals at the rates proposed by Peeters and Müller (2010) was therefore regarded as unlikely.

On the morning of 9 July, regarded as an ideal case because the OH reactivity was well explained and isoprene concentrations were low, we found a tendency for the models to underestimate HO_2(*), the opposite of the normal tendency of weak overestimation for HO_2(*). The underestimation, commonly found for the three LIF measurements, was associated with high NO conditions and was not explained by RO_2 interference. One possibility is that a missing HO_x source or regeneration process becomes important under these conditions, and this could influence our understanding of ozone production regimes.

Supplementary material related to this article is available online at: http://www.atmos-chem-phys.net/12/2567/2012/acp-12-2567-2012-supplement.pdf.

Acknowledgements. Helpful comments by two anonymous reviewers are greatly appreciated. This work was supported by the EU FP-6 program EUROCHAMP (grant no. RII3-CT-2004-505968), ACCENT (Priority 1.1.6.3. *Global Change and Ecosystems*, grant no. GOCE-CT-2004-505337), a Grant-in-Aid for Scientific Research (KAKENHI) (B) 22310018 and RR2002 of the Kyosei Project by the Ministry of Education, Science, Sports, and Culture of Japan. We thank F. J. Johnen for assistance with the experiments and K. D. Lu for discussions.

Edited by: P. O. Wennberg

References

Ammann, C., Spirig, C., Neftel, A., Steinbacher, M., Komenda, M., Schaub, A.: Application of PTR-MS for measurements of biogenic VOC in a deciduous forest, Int. J. Mass Spectrom., 239, 87–101, 2004.

Archibald, A. T., Cooke, M. C., Utembe, S. R., Shallcross, D. E., Derwent, R. G., and Jenkin, M. E.: Impacts of mechanistic changes on HOx formation and recycling in the oxidation of isoprene, Atmos. Chem. Phys., 10, 8097–8118, doi:10.5194/acp-10-8097-2010, 2010.

Berresheim, H., Elste, T., Plass-Dülmer, C., Eisele, F. L., Tanner, D. J.: Chemical ionization mass spectrometer for long-term measurements of atmospheric OH and H_2SO_4, Int. J. Mass Spectrom., 202, 91–109, doi:10.1016/S1387-3806(00)00233-5, 2000.

Brasseur, G., Hauglustaine, D., Walters, S., Rasch, R., Müller, J.-F., Granier, C., and Tie, X.: MOZART, a global chemical transport model for ozone and related chemical tracers 1. Model description, J. Geophys. Res., 103, 28265–28289, 1998.

Carslaw, N., Creasey, D. J., Harrison, D., Heard, D.E., Hunter, M.C., Jacobs, P. J., Jenkin, M. E., Lee, J. D., Lewis, A. C., Pilling, M. J., Saunders, S. M., and Seakins, P. W.: OH and HO_2 radical chemistry in a forested region of north-western Greece, Atmos. Environ., 35, 4725–4737, 2001.

Crounse, J. D., Paulot, F., Kjaergaard, H. G., and Wennberg, P. O.: Peroxy radical isomerization in the oxidation of isoprene, Phys. Chem. Chem. Phys., 13, 13607–13613, doi:10.1039/C1CP21330J, 2011.

Di Carlo, P., Brune, W. H., Martinez, M., Harder, H., Lesher, R., Ren, X., Thornberry, T., Carroll, M. A., Young, V., Shepson, P. B., Riemer, D., Apel, E., and Campbell, C.: Missing OH reactivity in a forest: Evidence for unknown reactive biogenic VOCs, Science, 304, 722–725, doi:10.1126/science.1094392, 2004.

Dillon, T. J.: Interactive comment on "Detection of HO_2 by laser-induced fluorescence: calibration and interferences from RO_2 radicals" by H. Fuchs et al., Atmos. Meas. Tech. Discuss., 4, C210–C213, 2011.

Dillon, T. J. and Crowley, J. N.: Direct detection of OH formation in the reactions of HO_2 with $CH_3C(O)O_2$ and other substituted peroxy radicals, Atmos. Chem. Phys., 8, 4877–4889, doi:10.5194/acp-8-4877-2008, 2008.

Elshorbany, Y. F., Kleffmann, J., Hofzumahaus, A., Kurtenbach, R., Wiesen, P., Brauers, T., Bohn, B., Dorn, H.-P., Fuchs, H., Holland, F., Rohrer, F., Tillmann, R., Wegener, R., Wahner, A., Kanaya, Y., Yoshino, A., Nishida, S., Kajii, Y. J., Martinez, M., Kubistin, D., Harder, H., Lelieveld, J., Elste, T., Plass-Dülmer, C., Stange, G., Berresheim, H., and Schurath, U.: HOx budgets during HO_xComp: A case study of HO_x chemistry under NO_x-limited conditions, J. Geophys. Res., 117, D03307, doi:10.1029/2011JD017008, 2012.

Fuchs, H., Brauers, T., Dorn, H.-P., Harder, H., Häseler, R., Hofzumahaus, A., Holland, F., Kanaya, Y., Kajii, Y., Kubistin, D., Lou, S., Martinez, M., Miyamoto, K., Nishida, S., Rudolf, M., Schlosser, E., Wahner, A., Yoshino, A., and Schurath, U.: Technical Note: Formal blind intercomparison of HO_2 measurements in the atmosphere simulation chamber SAPHIR during the HO_xComp campaign, Atmos. Chem. Phys., 10, 12233–12250, doi:10.5194/acp-10-12233-2010, 2010.

Fuchs, H., Bohn, B., Hofzumahaus, A., Holland, F., Lu, K. D., Nehr, S., Rohrer, F., and Wahner, A.: Detection of HO_2 by laser-induced fluorescence: calibration and interferences from RO_2 radicals, Atmos. Meas. Tech., 4, 1209–1225, doi:10.5194/amt-4-1209-2011, 2011.

Heland, J., Kleffmann, J., Kurtenbach, R., and Wiesen, P.: A New Instrument to Measure Gaseous Nitrous Acid (HONO) in the Atmosphere, Environ. Sci. Technol., 35, 3207–3212, 2001.

Hofzumahaus, A., Rohrer, F., Lu, K., Bohn, B., Brauers, T., Chang, C.-C., Fuchs, H., Holland, F., Kita, K., Kondo, Y., Li, X., Lou, S., Shao, M., Zeng, L., Wahner, A., and Zhang, Y.: Amplified Trace Gas Removal in the Troposphere, Science, 324, 1702–1704, doi:10.1126/science.1164566, 2009.

Kanaya, Y. and Akimoto, H.: Radicals in the marine boundary layer: Testing the current tropospheric chemistry mechanism, The Chemical Record, 2, 199–211, 2002.

Kanaya, Y. and Akimoto, H.: Gating a channel photomultiplier using a fast high voltage switch: Reduction of afterpulse rates in a laser-induced fluorescence instrument for measurement of atmospheric OH radical concentrations, Appl. Opt., 45, 1254–1259, 2006.

Kanaya, Y., Sadanaga, Y., Hirokawa, J., Kajii, Y., and Akimoto, H.: Development of a ground-based LIF instrument for measuring HO_x radicals: Instrumentation and calibrations, J. Atmos. Chem., 38, 73–110, doi:10.1023/A:1026559321911, 2001.

Kanaya, Y., Yokouchi, Y., Matsumoto, J., Nakamura, K., Kato, S., Tanimoto, H., Furutani, H., Toyota, K., and

Akimoto, H.: Implications of iodine chemistry for daytime HO_2 levels at Rishiri Island, Geophys. Res. Lett., 29, 1212, doi:10.1029/2001GL014061, 2002.

Kanaya, Y., Cao, R., Kato, S., Miyakawa, Y., Kajii, Y., Tanimoto, H., Yokouchi, Y., Mochida, M., Kawamura, K., and Akimoto, H.: Chemistry of OH and HO_2 radicals observed at Rishiri Island, Japan, in September 2003: Missing daytime sink of HO_2 and positive nighttime correlations with monoterpenes, J. Geophys. Res., 112, D11308, doi:10.1029/2006JD007987, 2007a.

Kanaya, Y., Cao, R., Akimoto, H., Fukuda, M., Komazaki, Y., Yokouchi, Y., Koike, M., Tanimoto, H., Takegawa, N., and Kondo, Y.: Urban photochemistry in central Tokyo: 1. Observed and modeled OH and HO_2 radical concentrations during the winter and summer of 2004, J. Geophys. Res., 112, D21312, doi:10.1029/2007JD008670, 2007b.

Kleffmann, J., Gavriloaiei, T., Hofzumahaus, A., Holland, F., Koppmann, R., Rupp, L., Schlosser, E., Siese, M., and Wahner, A.: Daytime formation of nitrous acid: A major source of OH radicals in a forest, Geophys. Res. Lett., 32, L05818, doi:10.1029/2005GL022524, 2005.

Komenda, M., Schaub, A., and Koppmann, R.: Description and characterization of an on-line system for long-term measurements of isoprene, methyl vinyl ketone, and methacrolein in ambient air, J. Chromat. A, 995, 185–201, 2003.

Kubistin, D., Harder, H., Martinez, M., Rudolf, M., Sander, R., Bozem, H., Eerdekens, G., Fischer, H., Gurk, C., Klüpfel, T., Königstedt, R., Parchatka, U., Schiller, C. L., Stickler, A., Taraborrelli, D., Williams, J., and Lelieveld, J.: Hydroxyl radicals in the tropical troposphere over the Suriname rainforest: comparison of measurements with the box model MECCA, Atmos. Chem. Phys., 10, 9705–9728, doi:10.5194/acp-10-9705-2010, 2010.

Lelieveld, J., Butler, T. M., Crowley, J., Dillon, T., Fischer, H., Ganzeveld, L., Harder, H., Lawrence, M. G., Martinez, M., Taraborrelli, D., and Williams, J.: Atmospheric oxidation capacity sustained by a tropical forest, Nature, 452, 737–740, doi:10.1038/nature06870, 2008.

Lu, K. D., Rohrer, F., Holland, F., Fuchs, H., Bohn, B., Brauers, T., Chang, C. C., Häseler, R., Hu, M., Kita, K., Kondo, Y., Li, X., Lou, S. R., Nehr, S., Shao, M., Zeng, L. M., Wahner, A., Zhang, Y. H., and Hofzumahaus, A.: Observation and modelling of OH and HO_2 concentrations in the Pearl River Delta 2006: a missing OH source in a VOC rich atmosphere, Atmos. Chem. Phys., 12, 1541–1569, doi:10.5194/acp-12-1541-2012, 2012.

Martinez, M., Harder, H., Kovacs, T. A., Simpas, J. B., Bassis, J., Lesher, R., Brune, W. H., Frost, G. J., Willians, E. J., Stroud, C. A., Jobson, B. T., Roberts, J. M., Hall, S. R., Shetter, R. E., Wert, B., Fried, A., Akicke, B., Stutz, J., Young, V. L., White, A. B., and Zamora, R. J.: OH and HO_2 concentrations, sources, and loss rates during the Southern Oxidants Study in Nashville, Tennessee, summer 1999, J. Geophys. Res., 108, 4617, doi:10.1029/2003JD003551, 2003.

Martinez, M., Harder, H., Kubistin, D., Rudolf, M., Bozem, H., Eerdekens, G., Fischer, H., Klüpfel, T., Gurk, C., Königstedt, R., Parchatka, U., Schiller, C. L., Stickler, A., Williams, J., and Lelieveld, J.: Hydroxyl radicals in the tropical troposphere over the Suriname rainforest: airborne measurements, Atmos. Chem. Phys., 10, 3759–3773, doi:10.5194/acp-10-3759-2010, 2010.

Mollner, A. K., Valluvadasan, S., Feng, L., Sprague, M. K., Okumura, M., Milligan, D. B., Bloss, W. J., Sander, S. P., Martien, P. T., Harley, R. A., McCoy, A. B., and Carter, W. P. L.: Rate of gas phase association of hydroxyl radical and nitrogen dioxide, Science, 330, 646–649, doi:10.1126/science.1193030, 2010.

Paulot, F., Crounse, J. D., Kjaergaard, H. G., Kürten, A., St. Clair, J. M., Seinfeld, J. H., and Wennberg, P. O.: Unexpected epoxide formation in the gas-phase photooxidation of isoprene, Science, 325, 730–733, doi:10.1126/science.1172910, 2009.

Peeters, J., Nguyen, T. L., and Vereecken, L.: HO_x radical regeneration in the oxidation of isoprene, Phys. Chem. Chem. Phys., 11, 5935–5939, doi:10.1039/b908511d, 2009.

Peeters, J. and Müller, J.-F.: HOx radical regeneration in isoprene oxidation via peroxy radical isomerisations, II: Experimental evidence and global impact, Phys. Chem. Chem. Phys., 12, 14227–14235, doi:10.1039/c0cp00811g, 2010.

Pöschl, U., von Kuhlmann, R., Poisson, N., and Crutzen, P. J.: Development and intercomparison of condensed isoprene oxidation mechanisms for global atmospheric modeling, J. Atmos. Chem., 37, 29–52, 2000.

Pugh, T. A. M., MacKenzie, A. R., Hewitt, C. N., Langford, B., Edwards, P. M., Furneaux, K. L., Heard, D. E., Hopkins, J. R., Jones, C. E., Karunaharan, A., Lee, J., Mills, G., Misztal, P., Moller, S., Monks, P. S., and Whalley, L. K.: Simulating atmospheric composition over a South-East Asian tropical rainforest: performance of a chemistry box model, Atmos. Chem. Phys., 10, 279–298, doi:10.5194/acp-10-279-2010, 2010.

Ravishankara, A. R., Dunlea, E. J., Blitz, M. A., Dillon, T. J., Heard, D. E., Pilling, M. J., Strekowski, R. S., Nicovich, J. M., and Wine, P. H.: Redetermination of the rate coefficient for the reaction of $O(^1D)$ with N_2, Geophys. Res. Lett., 29, 1745, doi:10.1029/2002GL014850, 2002.

Ren, X., Harder, H., Martinez, M., Lesher, R. L., Oliger, A., Simpas, J. B., Brune, W. H., Schwab, J. J., Demerjian, K. L., He, Y., Xhou, X., and Gao, H.: OH and HO_2 chemistry in the urban atmosphere of New York City, Atmos. Environ., 37(26), 3639–3651, 2003.

Ren, X., Brune, W. H., Mao, J., Mitchell, M. J., Lesher, R. L., Simpas, J. B., Metcalf, A. R., Schwab, J. J., Cai, C., Li, Y., Demerjian, K. L., Felton, H. D., Boynton, G., Adams, A., Perry, J., He. Y., Zhou, X., and Hou, J.: Behavior of OH and HO_2 in the winter atmosphere in New York City, Atmos. Environ., 40, S252–S263, 2006.

Ren, X., Olson, J. R., Crawford, J. H., Brune, W. H., Mao, J., Long, R. B., Chen, Z., Chen, G., Avery, M. A., Sachse, G. W., Barrick, J. D., Diskin, G. S., Huey, L. G., Fried, A., Cohen, R. C., Heikes, B., Wennberg, P. O., Singh, H. B., Blake, D. R., and Shetter, R. E.: HO_x chemistry during INTEX-A 2004: Observation, model calculation, and comparison with previous studies, J. Geophys. Res., 113, D05310, doi:10.1029/2007JD009166, 2008.

Rohrer, F. and Berresheim, H.: Strong correlation between levels of tropospheric hydroxyl radicals and solar ultraviolet radiation, Nature, 442, 7099, 184–187, doi:10.1038/nature04924, 2006.

Sadanaga, Y., Yoshino, A., Kato, S., and Kajii, Y.: Measurements of OH reactivity and photochemical ozone production in the urban atmosphere, Environ. Sci. Technol., 39, 8847–8852, 2005.

Sander, S. P., Friedl, R. R., Golden, D. M., Kurylo, M. J., Huie, R. E., Orkin, V. L., Mootgat, G. K., Ravishankara, A. R., Kolb, C. E., Molina, M. J., Finlayson-Pitts, B. J.: Chemical kinetics and photochemical data for use in stratospheric modeling, evaluation

number 14, JPL Publ. 02–25, Natl. Aeronaut. Space Admin., Jet Propul. Lab., Pasadena, Calif, 2003.

Schlosser, E., Brauers, T., Dorn, H.-P., Fuchs, H., Häseler, R., Hofzumahaus, A., Holland, F., Wahner, A., Kanaya, Y., Kajii, Y., Miyamoto, K., Nishida, S., Watanabe, K., Yoshino, A., Kubistin, D., Martinez, M., Rudolf, M., Harder, H., Berresheim, H., Elste, T., Plass-Dülmer, C., Stange, G., and Schurath, U.: Technical Note: Formal blind intercomparison of OH measurements: results from the international campaign HO_xComp, Atmos. Chem. Phys., 9, 7923–7948, doi:10.5194/acp-9-7923-2009, 2009.

Sommariva, R., Haggerstone, A.-L., Carpenter, L. J., Carslaw, N., Creasey, D. J., Heard, D. E., Lee, J. D., Lewis, A. C., Pilling, M. J., and Zádor, J.: OH and HO_2 chemistry in clean marine air during SOAPEX-2, Atmos. Chem. Phys., 4, 839–856, doi:10.5194/acp-4-839-2004, 2004.

Spirig, C., Neftel, A., Ammann, C., Dommen, J., Grabmer, W., Thielmann, A., Schaub, A., Beauchamp, J., Wisthaler, A., and Hansel, A.: Eddy covariance flux measurements of biogenic VOCs during ECHO 2003 using proton transfer reaction mass spectrometry, Atmos. Chem. Phys., 5, 465–481, doi:10.5194/acp-5-465-2005, 2005.

Stavrakou, T., Peeters, J., and Müller, J.-F.: Improved global modelling of HO_x recycling in isoprene oxidation: evaluation against the GABRIEL and INTEX-A aircraft campaign measurements, Atmos. Chem. Phys., 10, 9863–9878, doi:10.5194/acp-10-9863-2010, 2010.

Stockwell, W. R., Kirchner, F., Kuhn, M., and Seefeld, S.: A new mechanism for regional atmospheric chemistry modeling, J. Geophys. Res., 102(D22), 25847–25880, 1997.

Stone, D., Evans, M. J., Edwards, P. M., Commane, R., Ingham, T., Rickard, A. R., Brookes, D. M., Hopkins, J., Leigh, R. J., Lewis, A. C., Monks, P. S., Oram, D., Reeves, C. E., Stewart, D., and Heard, D. E.: Isoprene oxidation mechanisms: measurements and modelling of OH and HO_2 over a South-East Asian tropical rainforest during the OP3 field campaign, Atmos. Chem. Phys., 11, 6749–6771, doi:10.5194/acp-11-6749-2011, 2011.

Tan, D., Faloona, I., Simpas, J. B., Brune, W., Shepson, P. B., Couch, T. L., Sumner, A. L., Carroll, M. A., Thornberry, T., Apel, E., Riemer, D., Stockwell, W.: HO_x budgets in a deciduous forest: Results from the PROPHET summer 1998 campaign, J. Geophys. Res., 106, 24407–24427, 2001.

Taraborrelli, D., Lawrence, M. G., Butler, T. M., Sander, R., and Lelieveld, J.: Mainz Isoprene Mechanism 2 (MIM2): an isoprene oxidation mechanism for regional and global atmospheric modelling, Atmos. Chem. Phys., 9, 2751–2777, doi:10.5194/acp-9-2751-2009, 2009.

Wennberg, P. O., Hanisco, T. F., Jaeglé, L., Jacob, D. J., Hintsa, E. J., Lanzendorf, E. J., Anderson, J. G., Gao, R.-S., Keim, E. R., Donnelly, S. G., Del Negro, L. A., Fahey, D. W., McKeen, S. A., Salawitch, R. J., Webster, C. R., May, R. D., Herman, R. L., Proffitt, M. H., Margitan, J. J., Atlas, E. L., Schauffler, S. M., Flocke, F., McElroy, C. T., and Bui, T. P.: Hydrogen Radicals, Nitrogen Radicals, and the Production of O_3 in the Upper Troposphere, Science, 279, 49–53, doi:10.1126/science.279.5347.49, 1998.

Whalley, L. K., Edwards, P. M., Furneaux, K. L., Goddard, A., Ingham, T., Evans, M. J., Stone, D., Hopkins, J. R., Jones, C. E., Karunaharan, A., Lee, J. D., Lewis, A. C., Monks, P. S., Moller, S. J., and Heard, D. E.: Quantifying the magnitude of a missing hydroxyl radical source in a tropical rainforest, Atmos. Chem. Phys., 11, 7223–7233, doi:10.5194/acp-11-7223-2011, 2011.

Yoshino, A., Sadanaga, Y., Watanabe, K., Kato, S., Miyakawa, Y., Matsumoto, J., and Kajii, Y.: Measurement of total OH reactivity by laser-induced pump and probe technique – comprehensive observations in the urban atmosphere of Tokyo, Atmos. Environ., 40, 7869–7881, 2006.

Zhang, L., Brook, J. R., and Vet, R.: A revised parameterization for gaseous dry deposition in air-quality models, Atmos. Chem. Phys., 3, 2067–2082, doi:10.5194/acp-3-2067-2003, 2003.